

1 **Balancing sub- and supra-salt strain in salt-influenced rifts:**
2 **Implications for extension estimates**

3 Alexander J. Coleman^{a*}, Christopher A.-L. Jackson^a and Oliver B. Duffy^b

4
5 ^a Basins Research Group (BRG), Department of Earth Science and Engineering, Imperial College,
6 Prince Consort Road, London, SW7 2BP, UK.

7 ^b Bureau of Economic Geology, The University of Texas at Austin, University Station, Box X,
8 Austin, TX 78713-7508, USA.

9

10 *Corresponding Author: Alexander J. Coleman (a.coleman14@imperial.ac.uk)

11

12 **Keywords:** Salt-influenced rifting, strain balancing, normal faulting, Halten Terrace, extension
13 estimates, fault-related folding

14

15 **ABSTRACT**

16 The structural style of salt-influenced rifts may differ from those formed in predominantly brittle
17 crust. Salt can decouple sub- and supra-salt strain, causing sub-salt faults to be geometrically
18 decoupled from, but kinematically coupled to and responsible for, supra-salt forced folding. Salt-
19 influenced rifts thus contain more folds than their brittle counterparts, an observation often ignored
20 in extension estimates. Fundamental to determining whether sub- and supra-salt structures are
21 kinematically coherent, and the relative contributions of thin- (i.e. gravity-driven) and thick-
22 skinned (i.e. whole-plate stretching) deformation to accommodating rift-related strain, is our
23 ability to measure extension at both structural levels. We here use published physical models of

24 salt-influenced extension to show that line-length estimates yield more accurate values of sub- and
25 supra-salt extension compared to fault-heave, before applying these methods to seismic data from
26 the Halten Terrace, offshore Norway. We show that, given the abundance of ductile deformation
27 in salt-influenced rifts, significant amounts of extension may be ignored, leading to the erroneous
28 interpretations of thin-skinned, gravity-gliding. If a system is kinematically coherent, supra-salt
29 structures can help predict the occurrence and kinematics of sub-salt faults that may be poorly
30 imaged and otherwise poorly constrained.

31 **1. Introduction**

32 **1.1. Structural styles in salt-influenced rifts**

33 The structural style and evolution of rifts that contain rheological heterogeneities, such as
34 relatively thick salt (e.g. Hodgson et al., 1992; Stewart et al., 1996; Stewart et al., 1997; Pascoe et
35 al., 1999; Corfield and Sharp, 2000; Richardson et al., 2005; Kane et al., 2010; Duffy et al., 2013;
36 Wilson et al., 2015; Jackson and Lewis, 2016), may significantly differ from those forming in
37 predominantly ‘brittle’ crust (Fig. 1) (e.g. Gawthorpe and Leeder, 2000; Whipp et al., 2014; Duffy
38 et al., 2015). During the early stages of basement-involved extension in salt-influenced rifts, salt
39 may inhibit the upward propagation of sub-salt faults (Fig. 1b), mechanically decoupling them
40 from, but being responsible for, associated forced folds in supra-salt strata (e.g. Stearns, 1978;
41 Withjack et al., 1990; Maurin and Niviere, 1999; Duffy et al., 2013); such decoupling thus leads
42 to differing structural styles or a geometric disparity, above and below the intra-stratal detachment
43 (Jarrige, 1992). With increasing displacement, sub-salt faults may breach the folds and hard-link
44 with overlying, supra- salt faults (Koyi and Petersen, 1993; Harvey and Stewart, 1998; Withjack
45 and Callaway, 2000; Richardson et al., 2005; Kane et al., 2010). As extension continues, the degree

46 of vertical coupling increases and the geometric disparity between the fault populations decreases
47 between sub- and supra-salt strata (Pascoe et al., 1999; Dooley et al., 2003; Marsh et al., 2010).
48 Salt-influenced rifts therefore typically contain a greater degree of folding than those lacking an
49 intra-stratal detachment; the contribution of these folds in accommodating extensional strain,
50 especially within supra-salt strata, is often ignored.

51 *Insert Figure 1*

52 **1.1. Kinematic coherence**

53 Despite exhibiting different structural styles, sub- and supra-salt fault systems may form at the
54 same time and accommodate similar amounts of extension ('kinematic coherence' sensu Walsh
55 and Watterson, 1991) (Fig. 2). Field and seismic studies have shown that kinematic coherence can
56 be maintained between sub- and supra-salt fault systems over relatively long spatial ($10^1 - 10^3$ m;
57 (Walsh and Watterson, 1991; Childs et al., 1996; Giba et al., 2012; Long and Imber, 2012; Lewis
58 et al., 2013) and temporal scales (Walsh et al., 2003; Jackson and Larsen, 2009; Jackson and Lewis,
59 2016). The characteristics of such kinematically coherent systems are: (i) sub- and supra-salt
60 extension should balance (e.g. Richard, 1991; Stewart et al., 1996; Harvey and Stewart, 1998); (ii)
61 hard-linked faults may exist between the supra- and sub-salt units (e.g. Richard, 1991; Childs et
62 al., 1993; Koyi, 1993); (iii) individual fault displacement and timing are related to all others in the
63 array (Walsh and Watterson, 1991). Intra-stratal detachments can thus allow kinematic coherence
64 to be maintained between structures that, on first inspection, appear physically disconnected
65 (Gaullier et al., 1993; Childs et al., 1996; Stewart et al., 1996; Withjack and Callaway, 2000; Lewis
66 et al., 2013).

67 A key motivation for identifying whether sub- and supra salt deformation is kinematically
68 coherent is that once identified, it permits the use of supra-salt structures to constrain the timing

69 of sub-salt structures, as well as the mode (i.e. thick-skinned, whole-plate stretching vs. thin-
70 skinned, independent gravity-gliding) and magnitude of crustal extension. Determining the mode
71 of crustal extension has important tectono-stratigraphic implications, as the style, evolution and
72 distribution of supra-salt faults and folds control the distribution and geometry of syn-kinematic
73 depocentres (Gaullier et al., 1993; Stewart and Argent, 2000; Kane et al., 2010; Elliott et al., 2012;
74 Duffy et al., 2013; Mannie et al., 2014a; Mannie et al., 2014b; Mannie et al., 2016). In addition,
75 the stretching factor used in basin models for hydrocarbon exploration, is often measured in
76 seismic section, by measuring the magnitude of crustal extension (Marrett and Allmendinger,
77 1992; Stewart and Coward, 1995; Morley, 1996; Walsh et al., 1996). As such, accurately
78 constraining the amount, duration, and mode of crustal extension is critical for understanding heat
79 flow and the timing of source rock maturation in sedimentary basins (e.g. McKenzie, 1978;
80 Waples, 1998; Ritter et al., 2004; Van Wees et al., 2009).

81 *Insert Figure 2*

82 Fundamental to determining whether sub – and supra-salt fault systems balance is the ability to
83 accurately measure sub- and supra-salt strains. Prior work has shown that sub-salt fault
84 displacement does not always balance supra-salt fault displacement (Stewart and Coward, 1995;
85 Stewart et al., 1996; Stewart et al., 1997; Stewart, 2007). Although only a few studies have studied
86 strain partitioning below and above salt, we anticipate that the strain mismatch between sub- and
87 supra-salt strain could be attributed to: (i) sub-seismic deformation (Kautz and Sclater, 1988;
88 White, 1990), (ii) polyphase faulting (Stiros, 1991; Reston and McDermott, 2014; McDermott and
89 Reston, 2015), (iii) footwall erosion, which can produce an apparent reduction in fault heave
90 (Kusznir and Ziegler, 1992; Judge and Allmendinger, 2011), and (iv) inversion, which may reduce
91 the displacement measured along a pre-kinematic horizon (Stewart and Coward, 1995; Stewart et

92 al., 1996). By understanding sub- and supra-salt strain, important information on the tectonic
93 evolution of a salt-influenced rift can be determined, however, issues still remain regarding the
94 reliability of strain estimates in rifts and along individual fault systems. Of particular interest here,
95 is the hypothesis that this mismatch or strain discrepancy between sub- and supra salt strains can
96 be partly attributed to ductile strain (folding); an aspect hitherto largely ignored in previous studies
97 (e.g. Bishop et al., 1995; Stewart et al., 1996; Harvey and Stewart, 1998). Folding has been shown
98 to accommodate significant proportions of extension, in addition to brittle faulting, with the
99 relative proportions likely to vary between stratigraphic levels (Fig. 3) (Childs et al., 1996; Walsh
100 et al., 1996; Dooley et al., 2003; Long and Imber, 2012). Here, we follow the definition of strain
101 after Walsh et al. (1996) and define ‘ductile strain’ as a change in shape produced by structures too
102 small to be seismically imaged or represented individually on a given map or cross section by a
103 particular technique. ‘Brittle strains’ are defined as structural discontinuities that are resolvable
104 given a particular data type, such as fault offsets imaged in seismic reflection data.

105 *Insert Figure 3*

106 **1.2. Aims**

107 The aim of this paper is to determine the degree to which sub- and supra-salt fault and fold
108 systems are kinematically coherent, and, in a broader sense, how ductile cover deformation
109 influences extension estimates in salt-influenced rift basins. To achieve this, we first outline the
110 definitions we will employ throughout the remainder of the paper (Table 1), before answering the
111 following questions: (i) how does sub- and supra-salt structural style vary in salt-influenced rift
112 basins?; (ii) does fault-heave (which considers faulting only) or line-length (which considers both
113 faulting and folding) analysis produce more accurate estimates of sub- and supra-salt extension in
114 salt-influenced rift basins?; and (iii) how does our method of measuring extension influence our

115 ability to determine the degree of kinematic coherence between sub- and supra-salt fault systems?
116 We use two techniques to answer these questions. First, we apply the fault-heave and line-length
117 methods for estimating sub- and supra-salt extension to scaled physical models of salt-influenced
118 extension presented by Withjack and Callaway (2000). These models simulate the sub- and supra-
119 salt faulting and folding patterns, and in contrast to natural examples, the boundary conditions (e.g.
120 the true extension and supra-salt rheology) are known, allowing application and assessment of the
121 relative merits of the two methods for estimating extension in salt-influenced rifts. Second, we
122 apply the same methods for estimating extension to a 3D seismic survey from the Halten Terrace,
123 offshore Norway, to determine whether the supra-salt structural style is related to thick-skinned,
124 whole-plate stretching or thin-skinned, independent, gravity-driven deformation. The Halten
125 Terrace is covered by high-quality 3D and 2D seismic reflection data, which image three-
126 dimensional structural style of the sub- and supra-salt fault arrays. In addition, abundant well data,
127 tied to a regional stratigraphic framework, enables mapping of sub- and supra-salt strata to
128 constrain the timing of structural development. Given that the salt in this location is relatively thin
129 (c. 400 m) and immobile compared to other salt-influenced basins in the North Sea, diapirism is
130 minimal and no allochthonous salt bodies are developed, thereby permitting the study of salt-
131 influenced rift structures without significant structural overprinting. We show that sub- and supra-
132 salt structural styles can be significantly different, and that line-length analysis, which explicitly
133 considers folding as a key part of the extension-related strain, is more accurate than fault-heave
134 summation in calculating extension estimates in salt-influenced rifts. We find that, despite sub-
135 and supra-salt strata being extended by similar amounts and thus being kinematically coherent,
136 supra-salt strata preferentially accommodate strain by folding, whereas sub-salt strata tend to fault.
137 Our results highlight that kinematic coherence does not necessitate similar structural styles, and

138 fault arrays that are stratigraphically separated by salt should not be interpreted as being physically
139 or kinematically isolated.

140 *Insert Table 1*

141 **2. Dataset and Methods**

142 Two datasets were used to estimate extension in salt-influenced rift basins: (i) a series of
143 published dry sand and wet clay models of forced folds (Appendix A) (Withjack and Callaway,
144 2000), and (ii) a seismic reflection dataset from the Halten Terrace, offshore Norway. The physical
145 models were chosen as they were explicitly designed to simulate the incremental and finite
146 structural styles (e.g. faulting, forced folding) observed in salt-influenced rift basins, including the
147 Halten Terrace. However, unlike in most natural examples, which are relatively old and/or inactive,
148 the boundary conditions in the physical models (e.g. the system dimensions, total extension,
149 extension rate, etc.) are known. Furthermore, we can estimate the magnitude of extension from the
150 final models using different approaches, allowing any differences between the methods to be
151 quantified and evaluated. A full description of the physical models is provided by Withjack and
152 Callaway (2000); we provide only a brief summary of some of the key features (Table 2).

153 *Insert Table 2*

154 The physical models consist of three layers (Fig. 4) – a metal base that represents sub-salt strata,
155 an overlying silicone gel polymer that represents the salt, and an upper layer of either homogeneous
156 dry sand or wet clay, representing the sedimentary supra-salt. Localised cataclastic faulting was
157 the primary deformation style in the dry sand models (models 7, 8 and 9); as is common in such
158 dry sand models, ductile deformation, in the form of folding, was negligible. In contrast,
159 distributed cataclasis and folding was the primary deformation mechanism in the wet clay models

160 (Model 12); however, with increasing strain, deformation became more localised. During the
161 experiment (see Withjack and Callaway, 2000, for a full description), a constant downward
162 movement on a 45° dipping precut surface in the metal base simulated displacement along a single
163 sub-salt fault. With increasing slip, the silicone gel (salt) and the pre-kinematic (= pre-extension)
164 supra-salt were folded and then faulted, with subsiding areas being filled with sand or clay to
165 simulate syn-extension deposition. After each experiment, the models were sliced to create a series
166 of cross sections (Withjack and Callaway, 2000). We then measured the amount of extension in
167 each cross section using two approaches: (i) fault-heave summation, and (ii) line-length, and then
168 compared to the known values from Withjack and Callaway (2000), to evaluate their accuracy in
169 salt-influenced rift basins (Fig. 4). Fault-heave summation uses measured fault heaves along a pre-
170 kinematic horizon (Appendix D) and considers only brittle deformation (faulting) (e.g. Rouby et
171 al., 1996). Line-length analysis, measures the total unfaulted length of the same pre-kinematic
172 horizon, thus includes ductile (i.e. folding) and brittle strains. Errors for fault-heave summation
173 and line-length were calculated by measuring sections multiple times, taking note of the minimum
174 and maximum possible line-lengths and fault-heaves (see Appendix E for further details). Because
175 very small-scale and thus non-visible deformation is not included, both methods provide a
176 minimum estimate for extension (Marrett and Allmendinger, 1992; Burberry, 2015). This approach
177 allows us to compare two commonly employed approaches for estimating extension and to see
178 whether, in a kinematically coherent example (i.e. sub-salt = supra-salt extension), the extension
179 approaches used can be applied to the Halten Terrace natural example and evaluated. If an
180 additional extension episode has affected either the sub- or supra-salt strata, the measured amount
181 of extension will be greater. For example, if additional, thin-skinned gravity-driven deformation,
182 independent of whole-plate stretching has taken place, the extension will be greater in the supra-

183 salt compared to the sub-salt (Fig. 2 – unbalanced system). In contrast, if polyphase rifting has
184 occurred, then the sub-salt extension will be larger than that of the supra-salt.

185 *Insert Figure 4*

186 The seismic reflection data set consists of a 3D seismic survey and a series of 2D seismic lines
187 covering c. 3,200 km² of the Halten Terrace, offshore Norway (Fig. 5a-b), including the Midgard
188 and Smørbukk-Heidrun segments and the Grinda Graben (structural terminology after Koch and
189 Heum, 1995). The 3D and 2D seismic surveys are time-migrated and are zero-phase with European
190 Polarity (Brown, 2001). They have a record length of 6,000 ms. Inline and crossline spacing is
191 12.5 m for the 3D survey. The estimated vertical seismic resolution is c. 30 m, based on a mean
192 seismic frequency of c. 20 Hz and an average seismic velocity of c. 2,500 ms⁻¹, both of which were
193 measured within the depth range of interest (Appendix B-C). Eight wells, each containing a suite
194 of wireline logs (Appendix B), checkshots (Appendix C) and core-constrained formation tops,
195 were tied to the seismic data. Seismic reflection data was then depth-converted using a checkshot-
196 derived time-depth relationship (Appendix C). By tying the well and seismic data, we identified
197 seven key age-constrained pre- to post- salt seismic horizons: these were mapped to establish the
198 structural style for sub- and supra-salt strata (Fig. 6; Appendix B). We mapped >200 faults, which
199 were categorised as sub-, supra-salt restricted or through-going. The study area is divided into
200 three domains based on prominent along-strike changes in supra-salt fault strike: (i) northern
201 domain – NE-SW striking, (ii) central domain – N-S striking, and (iii) southern domain – NE-SW
202 striking (Fig. 7a-c). This allowed along-strike changes in structural style to be quantified. Finally,
203 we calculated extension perpendicular to the fault strike in each domain using the fault-heave
204 summation and line-length methods on the depth-converted seismic reflection data – the same
205 approach as used for the physical models from Withjack and Callaway (2000). To validate our

206 Halten Terrace interpretation, we restored a seismic section from the Halten Terrace (Appendix F)
207 by decompacting the overburden, untilting fault blocks back to horizontal, and unfolding horizons
208 using flexural slip (see Rowan and Ratliff, 2012; Lingrey and Vidal-Royo, 2015, for a full review
209 and details on structural restoration). Detailed information regarding all the datasets and methods
210 are included in Appendix E.

211 *Insert Figure 5-7*

212 **3. Estimating Extension in Sub- and Supra-salt Strata**

213 The restoration methodology described above (and in more detail in Appendix E) has been applied
214 to a series of physical models (models 7, 8, 9 and 12; Appendix A) published by Withjack and
215 Callaway (2000). In each model, the initial length (l_0), final length (l_1), and the amount of extension
216 is known (models 7, 8, 9 & 12; Table 3–6; Fig. 4) and can be compared with our measurements of
217 extension. Based on the likely magnitude of measurement error associated with both the fault-
218 heave and line-length methods, we anticipate an error of c. $\pm 1\%$ for measured extension. We also
219 note, in cases where fault-related folding is significant, fault-heave summation requires projection
220 of the footwall and hangingwall cut-offs (Appendix D); this may introduce a further c. $\pm 1\%$
221 measurement error for measured extension. This issue does not apply to the line-length method as
222 no stratal projection is required (see Appendix E for further details on uncertainties and errors).
223 Dry sand supra-salt strata in models 7, 8 and 9 do not thin during extension and, as a result, line-
224 length variations are negligible at the scale of observation. In contrast, wet clay supra-salt strata in
225 Model 12 thinned during extension, thus unit line-length is not preserved. Models 7, 8 and 12 all
226 contain supra-salt forced folds, whereas Model 9 does not: thus, by comparing extension estimates
227 by the different methods in examples both with, and without, supra-salt folding, we can ascertain

228 the relative the influence of folding on extension estimates in salt-influenced rifts. In all models,
229 sub-salt strata are faulted rather than folded.

230 *Insert Table 3-6*

231 All models had an initial length (l_0) of 330 mm, hence sub- and supra-salt strata had the same
232 initial line lengths and have been deformed by similar amounts; extension at both levels should
233 therefore balance. However, applying a fault-heave summation approach to models 7 and 8
234 produces a discrepancy in apparent extension between sub- and supra-salt strata, with the sub-salt
235 experiencing greater extension than the supra-salt. In contrast, when the line-length approach is
236 used, sub- and supra-salt extension broadly balance (discrepancy of <1%). Furthermore, different
237 approaches may yield different results (Fig. 4). For example, in models 7 and 8 (Table 3-4),
238 estimates of extension using line-length analysis are <50% larger than the fault-heave summation
239 approach, and similar to the known values, suggesting that folding may accommodate up to 50%
240 of the observable strain, similar to seismic-scale estimates by Walsh et al. (1996). In models
241 lacking appreciable folding (Model 9; Table 5), line-length and fault-heave estimates produce
242 similar extension values, and are comparable with known values. Where supra-salt strata are
243 largely ductile (Model 12; Table 6), line-length is not preserved during extension, due to thinning
244 related to stretching (Fig. 8), hence line-length and fault-heave summation underestimates the
245 amount of extension compared to the known values. Some of this underestimated extension, or
246 strain, is likely accommodated by non-visible or ‘cryptic’ deformation (Walsh et al., 1996; Butler
247 and Paton, 2010; Burberry, 2015) e.g. sub-granular deformation, and layer-parallel slip (Fig. 8).

248 *Insert Figure 8*

249 **4. Geological Setting of the Halten Terrace**

250 Having evaluated the two approaches for estimating extension in salt-influenced rifts i.e. fault-
251 heave summation and line-length, we can now apply these to a natural example, the Halten Terrace,
252 offshore Norway. The Halten Terrace is part of a large (c. 10,500 km² area), Devonian-to-Tertiary
253 extensional basin, located along the easternmost edge of the present Norwegian margin. It is
254 separated from the Trøndelag Platform to the east and the Midgard Segment to the NE by the
255 Bremstein Fault Complex, and from the deep Rås Basin in the west by the Klakk Fault Complex
256 (Fig. 5a). The structural framework and geological evolution of the Halten Terrace and
257 neighbouring areas are described in detail by Blystad (1995); and Bell et al. (2014); hence, in this
258 section, we provide only a brief review of the key tectonic and stratigraphic events such as to
259 provide the regional tectonostratigraphic and mechanostratigraphic context for our detailed study
260 of sub- and supra-salt fault populations (Fig. 6).

261 **4.1. Pre- Late Triassic**

262 The mid-Norwegian continental margin was subject to three periods (Early to Mid Devonian,
263 Carboniferous, and Late Permian to Early Triassic) of approximately E-W oriented extension
264 before the deposition of a Triassic salt layer (Blystad, 1995; Marsh et al., 2010). Rifting led to the
265 initial separation of Greenland from the western Norway, although the distribution and type of
266 associated structures and stratigraphy are all poorly constrained due to poor sub-salt seismic
267 imaging, a lack of deep (i.e. sub-salt) well penetrations, and younger halokinesis. On the Halten
268 Terrace, the deepest wells terminate in Triassic strata, including a thick sequence (<1 km) of
269 evaporites and shales, herein termed ‘salt’ (Jacobsen and van Veen, 1984). The salt was deposited
270 in an intra-rift subaerial basin in an arid climate, which became isolated during a regional sea-level
271 fall (Jacobsen and van Veen, 1984; Marsh et al., 2010).

272 **4.2. Post- Late Triassic**

273 During the latest Triassic–early Mid Jurassic, a <2 km thick, increasingly marine-influenced
274 overburden was deposited atop the salt (Corfield et al., 2001; Svela, 2001; Ichaso et al., 2016).
275 NW-SE oriented extension occurred in the late Mid Jurassic and continued into the Early
276 Cretaceous, eventually leading to the opening of the NE Atlantic Ocean in the Tertiary (Blystad,
277 1995; Corfield and Sharp, 2000; Richardson et al., 2005; Faleide et al., 2008; Marsh et al., 2010).
278 Below the salt, deformation was localised in NE-SW striking fault zones and was predominantly
279 brittle (Fig. 7). In contrast, above the salt, deformation was distributed in NE-SW trending broad,
280 $10^3 - 10^4$ m wide (ductile) folds with NE-SW striking supra-salt (brittle) normal faults detaching
281 onto the underlying salt, forming supra-salt restricted graben e.g. the Grinda Graben (Withjack et
282 al., 1990; Corfield and Sharp, 2000; Withjack and Callaway, 2000). It is these sub- and supra-salt
283 structures that we focus on in this study.

284 **5. Sub- and Supra-salt Structural Styles**

285 The Top Sub-salt and Top Ror Formation seismic horizons are used to define the sub- and supra-
286 salt structures of the Halten Terrace, respectively (Fig. 7a-b). An isochore of the Triassic Salt
287 interval delineates the distribution and geometry of salt structures (Fig. 9). Based on changes in
288 mean supra-salt fault strike, we split the sub- and supra-salt levels into the northern (NE-SW),
289 central (N-S) and southern (NE-SW) domains; this sub-division allows us to relate sub- and supra-
290 salt structural styles along strike. The key structures observed at sub- and supra-salt structural
291 levels are described below. In all cases, the faults are extensional unless otherwise stated.

292 *Insert Figure 9*

293 **5.1. Sub-salt**

294 At sub-salt levels, the Halten Terrace is characterised by a series of NE-SW to N-S striking (Fig.
295 7) fault blocks that are more deeply buried to the west (Fig. 10). The northern domain is dominated
296 by SE- and NW- dipping, dominantly NE-SW-striking sub-salt faults, with <1 km across-strike
297 spacing (Fig. 7b). Horst-graben structures are common, with the mean westward dip of the Top
298 Sub-salt being relatively steep (c. <7°). Fault throw ranges between 100 - 300 m in the east, and
299 increases to c. 500 m in the west. Sub-salt faults do not breach the overlying salt (Fig. 10a).

300 In the central domain, sub-salt faults strike N-S to NE-SW, with <4 - 6 km across-strike spacing
301 (Fig. 7b). Faults dominantly dip to the west (at c. 65°), and bound a series of fault blocks that
302 downstep to the west, with a steep regional dip (<7°). Faults throw is greatest in the east (<600 m),
303 with easternmost faults breaching the salt and supra-salt strata (Fig. 10b).

304 The southern domain is characterised by NE-SW striking normal faults, with typical across-
305 strike spacings of 5 – 10 km (Fig. 7b). Sub-salt faults bound a series of domino-style fault blocks
306 and horst-graben structures and do not link upwards with supra-salt faults. Here, faults range in
307 throw from 100 – 300 m, and typically dip westwards at c. 70°. The regional dip is relatively
308 shallow compared to the northern and central domains, and with the exception of fault block crests,
309 there is little relief at the Top Sub-salt level (Fig. 10c).

310 5.2. Salt

311 Triassic salt represents a major regional structural detachment (Fig. 9), thickening from (c. 100
312 – 200 m) in the east to >600 m in the west. Locally, substantial, abrupt changes in thickness and
313 top salt geometry occur, typically in association with sub- and supra-salt structural styles. For
314 example, salt is thickest in the immediate footwall of supra-salt faults (>200 m), and thinnest in
315 the hangingwalls (<100 m) (Fig. 10), forming salt rollers. In the north and south, the salt is broadly
316 isopachous with thicknesses of c. 200 – 500 m, and are not breached by hard-linked faults.

317 5.3. **Supra-salt**

318 The supra-salt strata (Fig. 7a) is deformed into a large (>18 km long by >15 km wide), NE-SW
319 to N-S trending, southerly plunging, NW-facing, fold. Fold amplitude increases northwards (from
320 500 to 800 m), with the fold becoming bisected by the 40 km long, up to 5 km wide, and NE-SW-
321 to N-S-trending Grinda Graben. Both the fold and the Grinda Graben overlie complex, sub-salt
322 relief (Fig. 7b). Despite displaying broadly similar NE-SW to N-S structural trends, supra-salt
323 strata are dominantly folded, whereas sub-salt strata are dominantly faulted.

324 In the northern domain, supra-salt faults strike N-S to NE-SW, are closely spaced (c. <1 – 3 km)
325 across-strike. The faults are planar and dip steeply (c. 60 - 80°) westwards, and have up to 700 m
326 of throw (Fig. 10a). The central domain is characterised by NNE-SSW striking faults that have a
327 typical across-strike spacing of 2 – 7 km. Most faults dip steeply (c. 60 – 70°) westwards, and are
328 planar – with increasing throw eastwards (from 120 – 400 m) (Fig. 10b). In the southern domain,
329 faults strike NE-SW, with a c. 2 – 6 km across-strike spacing. However, towards the south, faults
330 become more diffuse, becoming increasingly distributed into <2 km long segments. Faults are
331 typically listric, and dip towards the west (c. 50 - 75°), with typical throws of <50 - 200 m (Fig.
332 10c).

333 *Insert Figure 10*

334 **6. Balancing Sub- and Supra-salt Extension in the Halten Terrace**

335 Having established the differences in structural style between the predominantly faulted sub-
336 salt and folded and faulted supra-salt levels in the Halten Terrace, we now focus on the amount of
337 extension measured at both structural levels to investigate whether fault-heave or line-length is the
338 more effective technique for measuring extension in salt-influenced rifts, whether the sub- and

339 supra-salt structures are kinematically coherent, and if any thin-skinned, gravity-driven
340 deformation has taken place in the supra-salt strata, independent of thick-skinned, whole-plate
341 stretching.

342 Based on the likely measurement error associated with calculating extension on seismic
343 reflection profiles (see above and Appendix E), we anticipate a $\pm 6\%$ cumulative uncertainty in
344 values of extension using fault-heave summation, and a $\pm 4\%$ cumulative uncertainty associated
345 with line-length. Extension values derived from fault-heave summation have a greater uncertainty
346 than line-length (Fig. 7d-e), largely because of the projection of hangingwall and footwall cut-offs
347 (Appendix D) in geologically complex areas where larger degrees of extension are accommodated
348 by ductile strains (e.g. relay zones, near conjugate faults, within fault-related folds, etc; Walsh et
349 al., 1996). In addition, the degree of erosion, the choice of the pre-kinematic horizon and the cross
350 section to be measured will also affect the calculated extension (c. $\pm 1\%$ for line-length, c. $\pm 2\%$
351 for fault-heave) (see Appendix E for details).

352 Below the salt, extension measured solely from fault-heaves increases northwards, being highest
353 in the northern and central domains (c. 20 - 30 %) where sub- and supra-salt faults are hard-linked
354 (through-going). Above the salt, extension generally decreases southwards from c. 20% to 10%
355 (Fig. 7d). Across all the domains, supra-salt extension (average = 17%) is slightly less than sub-
356 salt extension (average = 24%).

357 In contrast, if folding and faulting are considered together and the line-length approach is used
358 (Fig. 7e), extension ranges from c. 10 – 20% for sub- and supra-salt levels, with the average sub-
359 and supra-salt extension being 13% and 12%, respectively. In the central domain, sub- and supra-
360 salt extension is similar (c. 20%); this contrasts with the results yielded by the fault-heave
361 summation method, where extension at the sub-salt level (c. 30%) was significantly larger than the

362 supra-salt level (c. 16%) (cf. Figs 7d and 7e). This suggests that folding accommodates a
363 significant amount of extension (e.g. Walsh and Watterson, 1991; Walsh et al., 1996; Long and
364 Imber, 2012). More specifically, in the Halten Terrace, folding may accommodate for as much as
365 half of the observable extension, a result similar to that obtained from the physical models (Table
366 3–4). In the northern and southern domains, supra-salt extension derived from line-length is
367 significantly larger (c. <12% larger) than its sub-salt counterpart, similar to the fault-heave
368 summation approach (Figs. 7d and e). Given that fault-heave summation only considers brittle
369 deformation along faults, and is similar to a line-length approach, it is likely that there is minimal
370 folding which would only be incorporated into line-length estimates. Furthermore, higher
371 extension in the supra-salt strata relative to the sub-salt could be attributed to thin-skinned, gravity-
372 driven deformation (e.g. Doré et al., 1997; Lundin and Doré, 1997; Welbon et al., 2007; Wilson et
373 al., 2013), that is independent of thick-skinned, whole-plate stretching. If so, updip extension
374 would need to be compensated by downdip shortening (e.g. salt-cored buckle folds) (Clausen and
375 Korstgård, 1996; Stewart and Argent, 2000; Rowan et al., 2004; Brun and Fort, 2011). However,
376 no such downdip shortening structures are observed, and so we suggest that it is more likely that
377 sub-salt extension is underestimated in the northern and southern domains; sub-salt faults outboard
378 of the study area (e.g. Fig. 5c shows a sub-salt fault outboard of the 3D survey) would balance the
379 supra-salt extension, as shown in physical models (Fig. 7 in Withjack and Callaway, 2000) (Fig.
380 7e).

381 For a sub- and supra-salt fault-fold system to be considered kinematically coherent, total
382 extension must be balanced, and the different levels must undergo deformation synchronously
383 (Walsh and Watterson, 1991). However, it is often difficult to know when sub-salt faults were
384 active. In most cases, this is related to: (i) low-quality, regional, 2D seismic reflection data, which

385 are unable to constrain the map-view geometry or displacement distribution along sub-salt faults,
386 (ii) a lack of borehole data that cannot demonstrate the spatial variations in salt rheology and
387 lithology, and their impact on the distribution and evolution of supra-salt structures, or (iii) a lack
388 of hard-linkage between sub- and supra-salt faults, hence there are no growth packages to constrain
389 sub-salt fault activity (Jackson and Lewis, 2016). Given that we interpret the fold overlying the
390 sub-salt faults in Figure 5c and Figure 10a-b as a forced fold (sensu Stearns, 1978), and observe
391 progressive onlapping by Upper Jurassic – Lower Cretaceous strata, we suggest that the sub-salt
392 faults were active during the Late Jurassic – Early Cretaceous. Given that line-length extension
393 across the domains is largely balanced (supra-salt average extension = 12%, sub-salt average
394 extension = 13%), and that sub- and supra-salt deformation was coeval, we suggest the system is
395 kinematically coherent and controlled principally by thick-skinned, whole-plate deformation.
396 Kinematic coherence is also supported by our kinematic restoration (see Appendix F). Our
397 conclusion is consistent with Richardson et al. (2005), who suggest that the salt was not thick
398 enough to fully decouple sub- and supra-salt strata, implying deformation would be linked in time
399 and space, and during the Late Jurassic and Early Cretaceous. An alternative although perhaps less
400 likely interpretation is that sub- and supra-salt deformation occurred at markedly different times
401 (i.e. sub-salt deformation = pre-Jurassic; supra-salt = Late Jurassic-to-Early Cretaceous), but were
402 coincidentally associated with similar magnitudes of extension (Jackson and Lewis, 2016).

403 **7. Discussion**

404 Our analysis of physical models of salt-influenced rifts and a natural example from the Halten
405 Terrace demonstrate that the choice of extension estimate approach (fault-heave summation vs.
406 line-length) can significantly affect extension estimates in salt-influenced rifts and, subsequently,

407 our ability to determine whether sub- and supra-salt deformation is kinematically coherent.
408 Furthermore, a reliance on fault-heave summation alone in folded supra-salt strata may lead to
409 inaccurate estimates of the amount of extension and the mode of crustal extension. In this section,
410 we discuss the wider implications of our study, with specific reference to: (i) sub- and supra-salt
411 structural style variability and coupling; (ii) the role of folding and faulting in accommodating
412 strain; and (iii) basin-scale estimates of rift-related extension and the identification of thin-skinned,
413 independent gravity-driven deformation and thick-skinned, whole-plate stretching.

414 **7.1. How does sub- and supra-salt structural style vary in salt-influenced rift basins?**

415 Structural styles in rift basins are not always the same above and below salt, and can change
416 through time (Harvey and Stewart, 1998; Richardson et al., 2005; Marsh et al., 2010). This is
417 common because salt can decouple sub- and supra-salt deformation, often with faulting below the
418 salt, and folding above the salt. At seismic-scale, supra-salt strata are largely folded, however, in
419 nature, supra-salt units may host closely-spaced ($10^1 - 10^2$ m scale) faults with relatively low throw
420 values (e.g. Withjack et al., 1990; Walsh et al., 1996; Patton et al., 1998; Sharp et al., 2000;
421 Withjack and Callaway, 2000; Jackson et al., 2006; Botter et al., 2014). Prior studies have
422 documented differences in structural style above and below salt, but have often considered each
423 mechanostratigraphic unit independently, and sometimes related variations in fault strike, polarity
424 and distribution to different modes of crustal extension (e.g. Coward and Stewart, 1995; Stewart
425 et al., 1996; Stewart et al., 1997; Harvey and Stewart, 1998; Stewart and Clark, 1999; Marsh et al.,
426 2010). Our results suggest that variations in sub- and supra-salt structural style does not mean
427 deformation are independent of one-another. Instead, we propose that if extension at both levels is
428 balanced, and folding is included, then it is likely that the deformation occurred synchronously

429 (i.e. different structural styles above and below salt can arise from the same deformation phase and
430 are related).

431 **7.2. Does a fault-heave summation or line-length approach lead to more accurate**
432 **extension estimates in salt-influenced rift basins?**

433 If sub- and supra-salt fault systems are developed at different times and due to independent
434 mechanisms, then the amount of extension in the sub- and supra-salt is also likely to differ. The
435 majority of studies have used fault-heave to estimate the horizontal extension in a 2D profile (e.g.
436 Gibbs, 1983; Ziegler, 1992; Wickham and Moeckel, 1997) and, although this may be reasonable
437 when studying basins lacking folding (Morley, 1996), this approach can lead to different extension
438 estimates in comparison to line-length methods. Given that folding is much more common in salt-
439 influenced rifts than basins without salt (e.g. Corfield and Sharp, 2000; Kane et al., 2010; Jackson
440 and Lewis, 2016), we have demonstrated here that it is essential to consider folding (ductile strain)
441 when estimating extension in salt-influenced extensional systems (Childs et al., 1995; Stewart and
442 Coward, 1995; Walsh et al., 1996; Withjack and Callaway, 2000; Long and Imber, 2010).

443 We prefer the line-length method to estimate extension in 2D sections in salt-influenced rifts as
444 faulting and folding are considered, and the approach has been shown to give more accurate
445 estimates of extension (and the stretching factor) than fault-heave summation. However, our results
446 show that line-length should not be used if supra-salt strata undergo thickness variations related to
447 stretching (e.g. Model 12 - Withjack and Callaway, 2000; Fig. 8). Stretching-related thickness
448 variations are most likely to occur in overpressured, ductile shales, and can be determined from
449 examination of seismic sections as well as in the field (e.g. boudinage, stretched clasts, foliation
450 subparallel to bedding) (e.g. Morley and Guerin, 1996; Morley and Naghadeh, 2016). It should be
451 noted that neither line-length nor fault-heave methods address factors such as internal shear and

452 differential compaction. In settings where such factors are deemed significant, a full structural
453 restoration, incorporating well data to constrain compositional and thus potential composition-
454 related variations in deformation process, is required for anything other than a first pass analysis.

455 **7.3. How does the choice of restoration method influence our ability to determine the**
456 **degree of coherence?**

457 Being able to accurately constrain the amount of extension in sub- and supra-salt strata is
458 important as it strongly influences how we interpret the processes driving deformation, helping
459 distinguish, for example, deformation related to thick-skinned, whole-plate stretching, or thin-
460 skinned, gravity-driven extension (gliding). Being able to determine the processes that have driven
461 deformation is critical for obtaining a sound understanding of basin evolution (fault patterns,
462 deformation rate, basin physiography), predicting the occurrence and activity of sub-salt faults and
463 supra-salt syn-rift sediment architecture and distribution. To even begin to determine the degree of
464 kinematic coherence between sub- and supra-salt faults, we need to be able to accurately estimate
465 extension. In salt-influenced rifts, we have shown that line-length is a more accurate approach
466 compared to fault-heave. Previous interpretations of the Halten Terrace have suggested that the
467 occurrence of supra-salt restricted fault blocks, detaching onto the salt and the position of pre-
468 kinematic horizons above a regional level (from regional 2D seismic lines) are a result of thin-
469 skinned, gravity-driven deformation (Welbon et al., 2007). However, by using the line-length
470 approach in this study, we propose that thick-skinned, whole-plate stretching is the process driving
471 deformation, corroborating interpretations by Pascoe et al. (1999) and Withjack et al. (1990).

472 Structural restorations (e.g. Lingrey and Vidal-Royo, 2015) and not simply line-length estimates
473 would be required to fully assess kinematic coherence across the Halten Terrace. However, when
474 comparing the results of a full restoration (Appendix F) with those arising from a line-length

475 approach, we find the result remains the same i.e. sub- and supra-salt deformation is still balanced,
476 and kinematically coherent. Furthermore, line-length is appropriate for assessing kinematic
477 coherence in relatively simple scenarios with moderate strain where bed-length preservation is a
478 reasonable assumption (Dahlstrom, 1969; Ramsay and Huber, 1987; Rowan and Ratliff, 2012;
479 Lingrey and Vidal-Royo, 2015). Where strain is very high and line-lengths are severely altered
480 with complex tectonic histories, or significant out-of-plane deformation has occurred, this simple
481 approach for estimating kinematic coherence may not be appropriate e.g. above diapir crests of the
482 Texas Gulf Coast (Rowan and Kligfield, 1989; Brewer et al., 1993) and the Southern North Sea
483 (Owen and Taylor, 1983), across rotated fault blocks of the Kwanza Basin (Rouby et al., 1993) and
484 within halite-rich units of the Levant Basin (Cartwright et al., 2012).

485 In kinematically coherent salt-influenced rifts, where sub-salt imaging may be poor, supra-salt
486 line-length extension estimates could be used to constrain thick-skinned, sub-salt extension, as
487 both levels are likely related to the same sequence of deformation events. Furthermore, supra-salt
488 structures could be used to constrain the likely occurrence and timing of activity of sub-salt
489 structures, and infer potential sub-salt reservoir compartmentalisation (e.g. Montgomery and
490 Moore, 1997; Uphoff, 2005). In addition, by calculating the timing and amount of extension in the
491 supra-salt strata, and hence the sub-salt strata, stretching factors can be calculated and the basement
492 heat flow may be modelled (see Van Wees et al., 2009 for a review of basement heat flow estimates
493 derived from stretching factors).

494 **8. Conclusions**

495 We have used a series of published dry sand and wet clay models of forced folds from Withjack
496 and Callaway (2000), and a high-quality seismic dataset across the Halten Terrace, offshore
497 Norway to show:

- 498 1. Structural styles above and below the salt may exhibit largely different structural styles,
499 albeit in the physical models or in the Halten Terrace, offshore Norway. Thick-skinned,
500 localised brittle faulting is dominant below the salt, while ductile flow occurs within the
501 overlying salt. Thick- and thin- skinned, brittle faulting and ductile folding is present within
502 the supra-salt strata.
- 503 2. When estimating extension in physical models, we show that line-length is more accurate
504 than fault-heave summation. This is largely attributed to a failure to include ductile strain
505 (folding) in fault-heave approaches, which is very common in salt-influenced rifts.
- 506 3. A failure to include folding, especially in salt-influenced rifts, may lead to erroneous
507 extension values, and may incorrectly suggest excess thin-skinned, gravity-gliding
508 independent of thick-skinned deformation. Furthermore, extension estimates, will
509 significantly affect the stretching factor utilised in basin models to predict basement heat
510 flow and the timing of source rock maturity.
- 511 4. The findings highlight that extension above and below the salt is largely similar in the
512 Halten Terrace despite different structural styles, indicative of kinematic coherence
513 between sub- and supra-salt structures; deformation at both levels likely occurred
514 synchronously, during the Mid Jurassic – Early Cretaceous rift phase.

515 5. When a system has similar amounts of extension above and below the salt, the supra- salt
516 structural style can be used to constrain the occurrence of sub-salt structures and estimate
517 the timing of thick-skinned extension that may otherwise be poorly constrained.

518 **Acknowledgements**

519 We would like to thank Schlumberger for the provision of the Petrel software licenses to
520 Imperial College London. In addition, Midland Valley are thanked for the Move software. The
521 Norwegian Petroleum Directorate (NPD), Statoil and PGS are thanked for the provision of data.
522 We extend our thanks to Gavin Elliott for Figure 1b, and to the Basins Research Group, especially,
523 Thomas B. Phillips, for their comments on earlier versions of this manuscript. Michael R. Hudec
524 and Tim P. Dooley are also thanked for their in-depth discussions regarding estimating extension
525 in salt provinces. We thank editor Ian Alsop, as well as Oskar Vidal-Royo and Peter Betts for
526 constructive reviews that greatly improved this manuscript.

527 **References**

- 528 Bell, R. E., Jackson, C. A. L., Elliott, G. M., Gawthorpe, R. L., Sharp, I. R., and Michelsen, L., 2014, Insights into the
529 development of major rift-related unconformities from geologically constrained subsidence modelling:
530 Halten Terrace, offshore mid Norway: Basin Research, v. 26, no. 1, p. 203-224.
- 531 Bishop, D. J., Buchanan, P. G., and Bishop, C. J., 1995, Gravity-driven thin-skinned extension above Zechstein Group
532 evaporites in the western central North Sea: an application of computer-aided section restoration techniques:
533 Marine and Petroleum Geology, v. 12, no. 2, p. 115-135.
- 534 Blystad, P., 1995, Structural Elements of the Norwegian Continental Shelf: The Norwegian Sea Region, Norwegian
535 Petroleum Directorate.
- 536 Botter, C., Cardozo, N., Hardy, S., Lecomte, I., and Escalona, A., 2014, From mechanical modeling to seismic imaging
537 of faults: A synthetic workflow to study the impact of faults on seismic: Marine and Petroleum Geology, v.
538 57, p. 187-207.
- 539 Brewer, R. C., and Groshong Jr, R. H., 1993, Restoration of cross sections above intrusive salt domes: AAPG Bulletin,
540 v. 77, no. 10, p. 1769-1780.
- 541 Brown, A. R., 2001, Calibrate yourself to your data! A vital first step in seismic interpretation: Geophysical
542 Prospecting, v. 49, no. 6, p. 729-733.
- 543 Brun, J.-P., and Fort, X., 2011, Salt tectonics at passive margins: Geology versus models: Marine and Petroleum
544 Geology, v. 28, no. 6, p. 1123-1145.
- 545 Burberry, C. M., 2015, Spatial and temporal variation in penetrative strain during compression: Insights from analog
546 models: Lithosphere, v. 7, no. 6, p. 611-624.

547 Butler, R., and Paton, D., 2010, Evaluating lateral compaction in deepwater fold and thrust belts: How much are we
548 missing from “nature’s sandbox”: *GSA Today*, v. 20, no. 3, p. 4-10.

549 Cartwright, J., Jackson, M., Dooley, T., and Higgins, S., 2012, Strain partitioning in gravity-driven shortening of a
550 thick, multilayered evaporite sequence: Geological Society, London, Special Publications, v. 363, no. 1, p.
551 449-470.

552 Childs, C., Easton, S. J., Vendeville, B. C., Jackson, M. P. A., Lin, S. T., Walsh, J. J., and Watterson, J., 1993, Kinematic
553 analysis of faults in a physical model of growth faulting above a viscous salt analogue: *Tectonophysics*, v.
554 228, no. 3–4, p. 313-329.

555 Childs, C., Nicol, A., Walsh, J. J., and Watterson, J., 1996, Growth of vertically segmented normal faults: *Journal of*
556 *Structural Geology*, v. 18, no. 12, p. 1389-1397.

557 Childs, C., Watterson, J., and Walsh, J. J., 1995, Fault overlap zones within developing normal fault systems: *Journal*
558 *of the Geological Society*, v. 152, no. 3, p. 535-549.

559 Clausen, O. R., and Korstgård, J. A., 1996, Planar detaching faults in the southern Horn Graben, Danish North sea:
560 *Marine and Petroleum Geology*, v. 13, no. 5, p. 537-548.

561 Corfield, S., and Sharp, I., 2000, Structural style and stratigraphic architecture of fault propagation folding in
562 extensional settings: a seismic example from the Smørbukk area, Halten Terrace, Mid-Norway: *Basin*
563 *Research*, v. 12, no. 3-4, p. 329-341.

564 Corfield, S., Sharp, I., Häger, K.-O., Dreyer, T., and Underhill, J., 2001, An integrated study of the garn and melke
565 formations (middle to upper jurassic) of the smorbukk area, halten terrace, mid-norway, *in* Ole, J. M., and
566 Tom, D., eds., *Norwegian Petroleum Society Special Publications*, Volume Volume 10, Elsevier, p. 199-210.

567 Coward, M., and Stewart, S., 1995, Salt-influenced structures in the Mesozoic-Tertiary cover of the southern North
568 Sea, UK.

569 Dahlstrom, C., 1969, Balanced cross sections: *Canadian Journal of Earth Sciences*, v. 6, no. 4, p. 743-757.

570 Dooley, T., McClay, K., and Pascoe, R., 2003, 3D analogue models of variable displacement extensional faults:
571 applications to the Revfallet Fault system, offshore mid-Norway: Geological Society, London, Special
572 Publications, v. 212, no. 1, p. 151-167.

573 Doré, A., Lundin, E., Fichler, C., and Olesen, O., 1997, Patterns of basement structure and reactivation along the NE
574 Atlantic margin: *Journal of the Geological Society*, v. 154, no. 1, p. 85-92.

575 Duffy, O. B., Bell, R. E., Jackson, C. A. L., Gawthorpe, R. L., and Whipp, P. S., 2015, Fault growth and interactions
576 in a multiphase rift fault network: Horda Platform, Norwegian North Sea: *Journal of Structural Geology*, v.
577 80, p. 99-119.

578 Duffy, O. B., Gawthorpe, R. L., Docherty, M., and Brocklehurst, S. H., 2013, Mobile evaporite controls on the
579 structural style and evolution of rift basins: Danish Central Graben, North Sea: *Basin Research*, v. 25, no. 3,
580 p. 310-330.

581 Elliott, G. M., Wilson, P., Jackson, C. A. L., Gawthorpe, R. L., Michelsen, L., and Sharp, I. R., 2012, The linkage
582 between fault throw and footwall scarp erosion patterns: an example from the Bremstein Fault Complex,
583 offshore Mid-Norway: *Basin Research*, v. 24, no. 2, p. 180-197.

584 Faleide, J. I., Tsikalas, F., Breivik, A. J., Mjelde, R., Ritzmann, O., Engen, O., Wilson, J., and Eldholm, O., 2008,
585 Structure and evolution of the continental margin off Norway and the Barents Sea: *Episodes*, v. 31, no. 1, p.
586 82-91.

587 Gaullier, V., Brun, J. P., Gue´rin, G., and Lecanu, H., 1993, Raft tectonics: the effects of residual topography below a
588 salt de´collement: *Tectonophysics*, v. 228, no. 3–4, p. 363-381.

589 Gawthorpe, R. L., and Leeder, M. R., 2000, Tectono-sedimentary evolution of active extensional basins: *Basin*
590 *Research*, v. 12, no. 3-4, p. 195-218.

591 Giba, M., Walsh, J. J., and Nicol, A., 2012, Segmentation and growth of an obliquely reactivated normal fault: *Journal*
592 *of Structural Geology*, v. 39, p. 253-267.

593 Gibbs, A. D., 1983, Balanced cross-section construction from seismic sections in areas of extensional tectonics:
594 *Journal of Structural Geology*, v. 5, no. 2, p. 153-160.

595 Harvey, M. J., and Stewart, S. A., 1998, Influence of salt on the structural evolution of the Channel Basin: Geological
596 Society, London, Special Publications, v. 133, no. 1, p. 241-266.

597 Hodgson, N., Farnsworth, J., and Fraser, A., 1992, Salt-related tectonics, sedimentation and hydrocarbon plays in the
598 Central Graben, North Sea, UKCS: Geological Society, London, Special Publications, v. 67, no. 1, p. 31-63.

599 Ichaso, A. A., Dalrymple, R. W., and Martinius, A. W., 2016, Basin analysis and sequence stratigraphy of the synrift
600 Tilje Formation (Lower Jurassic), Halten terrace giant oil and gas fields, offshore mid-Norway: *AAPG*
601 *Bulletin*, v. 100, no. 8, p. 1329-1375.

602 Jackson, C.-L., and Larsen, E., 2009, Temporal and spatial development of a gravity-driven normal fault array:
603 Middle–Upper Jurassic, South Viking Graben, northern North Sea: *Journal of Structural Geology*, v. 31, no.
604 4, p. 388-402.

605 Jackson, C. A. L., Gawthorpe, R. L., and Sharp, I. R., 2006, Style and sequence of deformation during extensional
606 fault-propagation folding: examples from the Hammam Faraun and El-Qaa fault blocks, Suez Rift, Egypt:
607 *Journal of Structural Geology*, v. 28, no. 3, p. 519-535.

608 Jackson, C. A. L., and Lewis, M. M., 2016, Structural style and evolution of a salt-influenced rift basin margin; the
609 impact of variations in salt composition and the role of polyphase extension: *Basin Research*, v. 28, no. 1, p.
610 81-102.

611 Jacobsen, V. W., and van Veen, P., 1984, The Triassic offshore Norway north of 62 N, *Petroleum geology of the north*
612 *European margin*, Springer, p. 317-327.

613 Jarrige, J.-J., 1992, Variation in extensional fault geometry related to heterogeneities within basement and sedimentary
614 sequences: *Tectonophysics*, v. 215, no. 1, p. 161-166.

615 Judge, P. A., and Allmendinger, R. W., 2011, Assessing uncertainties in balanced cross sections: *Journal of Structural*
616 *Geology*, v. 33, no. 4, p. 458-467.

617 Kane, K. E., Jackson, C. A. L., and Larsen, E., 2010, Normal fault growth and fault-related folding in a salt-influenced
618 rift basin: South Viking Graben, offshore Norway: *Journal of Structural Geology*, v. 32, no. 4, p. 490-506.

619 Kautz, S. A., and Sclater, J. G., 1988, Internal deformation in clay models of extension by block faulting: *Tectonics*,
620 v. 7, no. 4, p. 823-832.

621 Koch, J.-O., and Heum, O., 1995, Exploration trends of the Halten Terrace: *Norwegian Petroleum Society Special*
622 *Publications*, v. 4, p. 235-251.

623 Koyi, H., 1993, The effect of basement faulting on diapirism: *Journal of Petroleum Geology*, v. 16, no. 3, p. 285-312.

624 Koyi, H., and Petersen, K., 1993, Influence of basement faults on the development of salt structures in the Danish
625 Basin: *Marine and Petroleum Geology*, v. 10, no. 2, p. 82-94.

626 Kuszniir, N., and Ziegler, P., 1992, The mechanics of continental extension and sedimentary basin formation: a simple-
627 shear/pure-shear flexural cantilever model: *Tectonophysics*, v. 215, no. 1, p. 117-131.

628 Lewis, M. M., Jackson, C. A. L., and Gawthorpe, R. L., 2013, Salt-influenced normal fault growth and forced folding:
629 The Stavanger Fault System, North Sea: *Journal of Structural Geology*, v. 54, p. 156-173.

630 Lingrey, S., and Vidal-Royo, O., 2015, Evaluating the quality of bed length and area balance in 2D structural
631 restorations: *Interpretation*, v. 3, no. 4, p. SAA133-SAA160.

632 Long, J., and Imber, J., 2010, Geometrically coherent continuous deformation in the volume surrounding a seismically
633 imaged normal fault-array: *Journal of Structural Geology*, v. 32, no. 2, p. 222-234.

634 Long, J. J., and Imber, J., 2012, Strain compatibility and fault linkage in relay zones on normal faults: *Journal of*
635 *Structural Geology*, v. 36, p. 16-26.

636 Lundin, E., and Doré, A., 1997, A tectonic model for the Norwegian passive margin with implications for the NE
637 Atlantic: Early Cretaceous to break-up: *Journal of the Geological Society*, v. 154, no. 3, p. 545-550.

638 Mannie, A. S., Jackson, C. A.-L., and Hampson, G. J., 2014a, Shallow-marine reservoir development in extensional
639 diapir-collapse minibasins: An integrated subsurface case study from the Upper Jurassic of the Cod terrace,
640 Norwegian North Sea: *AAPG Bulletin*, v. 98, no. 10, p. 2019-2055.

641 Mannie, A. S., Jackson, C. A.-L., Hampson, G. J., and Fraser, A. J., 2016, Tectonic controls on the spatial distribution
642 and stratigraphic architecture of a net-transgressive shallow-marine synrift succession in a salt-influenced rift
643 basin: Middle to Upper Jurassic, Norwegian Central North Sea: *Journal of the Geological Society*, p. jgs2016-
644 2033.

645 Mannie, A. S., Jackson, C. A. L., and Hampson, G. J., 2014b, Structural controls on the stratigraphic architecture of
646 net-transgressive shallow-marine strata in a salt-influenced rift basin: Middle-to-Upper Jurassic Egersund
647 Basin, Norwegian North Sea: *Basin Research*, v. 26, no. 5, p. 675-700.

648 Marrett, R., and Allmendinger, R. W., 1992, Amount of extension on "small" faults: An example from the Viking
649 graben: *Geology*, v. 20, no. 1, p. 47-50.

650 Marsh, N., Imber, J., Holdsworth, R., Brockbank, P., and Ringrose, P., 2010, The structural evolution of the Halten
651 Terrace, offshore Mid-Norway: extensional fault growth and strain localisation in a multi-layer brittle–ductile
652 system: *Basin Research*, v. 22, no. 2, p. 195-214.

653 Maurin, J. C., and Nivière, B., 1999, Extensional forced folding and decollement of the pre-rift series along the Rhine
654 graben and their influence on the geometry of the syn-rift sequences: *Geological Society, London, Special*
655 *Publications*, v. 169, no. 1, p. 73-86.

656 McDermott, K., and Reston, T., 2015, To see, or not to see? Rifted margin extension: *Geology*, v. 43, no. 11, p. 967-
657 970.

658 McKenzie, D., 1978, Some remarks on the development of sedimentary basins: *Earth and Planetary science letters*, v.
659 40, no. 1, p. 25-32.

660 Montgomery, S. L., and Moore, D., 1997, Subsalt play, Gulf of Mexico: a review: *AAPG bulletin*, v. 81, no. 6, p. 871-
661 896.

662 Morley, C., 1996, Discussion of potential errors in fault heave methods for extension estimates in rifts, with particular
663 reference to fractal fault populations and inherited fabrics: *Geological Society, London, Special Publications*,
664 v. 99, no. 1, p. 117-134.

665 Morley, C., and Guerin, G., 1996, Comparison of gravity-driven deformation styles and behavior associated with
666 mobile shales and salt: *Tectonics*, v. 15, no. 6, p. 1154-1170.

667 Morley, C. K., and Naghadeh, D. H., 2016, Tectonic compaction shortening in toe region of isolated listric normal
668 fault, North Taranaki Basin, New Zealand: *Basin Research*, p. n/a-n/a.

669 Owen, P., and Taylor, N., 1983, A salt pillow structure in the southern North Sea: *Seismic expressions of structural*
670 *styles: AAPG Studies in geology series*, no. 15.

671 Pascoe, R., Hooper, R., Storhaug, K., and Harper, H., Evolution of extensional styles at the southern termination of
672 the Nordland Ridge, Mid-Norway: a response to variations in coupling above Triassic salt, *in Proceedings*
673 *Geological Society, London, Petroleum Geology Conference series 1999, Volume 5, Geological Society of*
674 *London*, p. 83-90.

675 Patton, T. L., Logan, J. M., and Friedman, M., 1998, Experimentally generated normal faults in single-layer and
676 multilayer limestone specimens at confining pressure: *Tectonophysics*, v. 295, no. 1, p. 53-77.

677 Ramsay, J. G., and Huber, M. I., 1987, *The techniques of modern structural geology*, Academic press.

678 Reston, T., and McDermott, K., 2014, An assessment of the cause of the ‘extension discrepancy’ with reference to the
679 west Galicia margin: *Basin Research*, v. 26, no. 1, p. 135-153.

680 Richard, P., 1991, Experiments on faulting in a two-layer cover sequence overlying a reactivated basement fault with
681 oblique-slip: *Journal of Structural Geology*, v. 13, no. 4, p. 459-469.

682 Richardson, N. J., Underhill, J. R., and Lewis, G., 2005, The role of evaporite mobility in modifying subsidence
683 patterns during normal fault growth and linkage, Halten Terrace, Mid-Norway: *Basin Research*, v. 17, no. 2,
684 p. 203-223.

685 Ritter, U., Zielinski, G. W., Weiss, H. M., Zielinski, R. L. B., and Sættem, J., 2004, Heat flow in the Vøring Basin,
686 Mid-Norwegian Shelf: *Petroleum Geoscience*, v. 10, no. 4, p. 353-365.

687 Rouby, D., Cobbold, P. R., Szatmari, P., Demercian, S., Coelho, D., and Rici, J. A., 1993, Least-squares palinspastic
688 restoration of regions of normal faulting—application to the Campos basin (Brazil): *Tectonophysics*, v. 221,
689 no. 3, p. 439-452.

690 Rouby, D., Fossen, H., and Cobbold, P. R., 1996, Extension, displacement, and block rotation in the larger Gullfaks
691 area, northern North Sea: determined from map view restoration: *AAPG bulletin*, v. 80, no. 6, p. 875-889.

692 Rowan, M. G., and Kligfield, R., 1989, Cross section restoration and balancing as aid to seismic interpretation in
693 extensional terranes: *AAPG bulletin*, v. 73, no. 8, p. 955-966.

694 Rowan, M. G., Peel, F. J., and Vendeville, B. C., 2004, Gravity-driven fold belts on passive margins.

695 Rowan, M. G., and Ratliff, R. A., 2012, Cross-section restoration of salt-related deformation: Best practices and
696 potential pitfalls: *Journal of Structural Geology*, v. 41, p. 24-37.

697 Sharp, I., Gawthorpe, R., Armstrong, B., and Underhill, J., 2000, Propagation history and passive rotation of mesoscale
698 normal faults: implications for synrift stratigraphic development: *Basin Research*, v. 12, no. 3-4, p. 285-305.

699 Stearns, D. W., 1978, Faulting and forced folding in the Rocky Mountains foreland: *Geological Society of America*
700 *Memoirs*, v. 151, p. 1-38.

701 Stewart, S., 2007, Salt tectonics in the North Sea Basin: a structural style template for seismic interpreters: *SPECIAL*
702 *PUBLICATION-GEOLOGICAL SOCIETY OF LONDON*, v. 272, p. 361.

703 Stewart, S., and Argent, J., 2000, Relationship between polarity of extensional fault arrays and presence of
704 detachments: *Journal of Structural Geology*, v. 22, no. 6, p. 693-711.

705 Stewart, S. A., and Clark, J. A., 1999, Impact of salt on the structure of the Central North Sea hydrocarbon fairways:
706 *Geological Society, London, Petroleum Geology Conference Series*, v. 5, p. 179-200.

707 Stewart, S. A., and Coward, M. P., 1995, Synthesis of salt tectonics in the southern North Sea, UK: *Marine and*
708 *Petroleum Geology*, v. 12, no. 5, p. 457-475.

709 Stewart, S. A., Harvey, M. J., Otto, S. C., and Weston, P. J., 1996, Influence of salt on fault geometry: examples from
710 the UK salt basins: *Geological Society, London, Special Publications*, v. 100, no. 1, p. 175-202.

711 Stewart, S. A., Ruffell, A. H., and Harvey, M. J., 1997, Relationship between basement-linked and gravity-driven fault
712 systems in the UKCS salt basins: *Marine and Petroleum Geology*, v. 14, no. 5, p. 581-604.

713 Stiros, S., 1991, Heat flow and thermal structure of the Aegean Sea and the Southern Balkans, *Terrestrial Heat Flow*
714 *and the Lithosphere Structure*, Springer, p. 395-416.

715 Svela, K. E., 2001, Sedimentary facies in the fluvial-dominated Åre formation as seen in the Åre 1 member in the
716 heidrun field, *in* Ole, J. M., and Tom, D., eds., *Norwegian Petroleum Society Special Publications*, Volume
717 Volume 10, Elsevier, p. 87-102.

718 Uphoff, T. L., 2005, Subsalt (pre-Jurassic) exploration play in the northern Lusitanian basin of Portugal: *AAPG*
719 *bulletin*, v. 89, no. 6, p. 699-714.

720 Van Wees, J. D., van Bergen, F., David, P., Nepveu, M., Beekman, F., Cloetingh, S., and Bonté, D., 2009, Probabilistic
721 tectonic heat flow modeling for basin maturation: Assessment method and applications: *Marine and*
722 *Petroleum Geology*, v. 26, no. 4, p. 536-551.

723 Walsh, J., Bailey, W., Childs, C., Nicol, A., and Bonson, C., 2003, Formation of segmented normal faults: a 3-D
724 perspective: *Journal of Structural Geology*, v. 25, no. 8, p. 1251-1262.

725 Walsh, J. J., and Watterson, J., 1991, Geometric and kinematic coherence and scale effects in normal fault systems:
726 *Geological Society, London, Special Publications*, v. 56, no. 1, p. 193-203.

727 Walsh, J. J., Watterson, J., Childs, C., and Nicol, A., 1996, Ductile strain effects in the analysis of seismic
728 interpretations of normal fault systems: *Geological Society, London, Special Publications*, v. 99, no. 1, p. 27-
729 40.

730 Waples, D. W., 1998, *Basin modelling: how well have we done?: Geological Society, London, Special Publications*,
731 v. 141, no. 1, p. 1-14.

732 Welbon, A. I. F., Brockbank, P. J., Brunnsden, D., and Olsen, T. S., 2007, *Characterizing and producing from reservoirs*
733 *in landslides: challenges and opportunities: Geological Society, London, Special Publications*, v. 292, no. 1,
734 p. 49-74.

735 Whipp, P., Jackson, C., Gawthorpe, R., Dreyer, T., and Quinn, D., 2014, Normal fault array evolution above a
736 reactivated rift fabric; a subsurface example from the northern Horda Platform, Norwegian North Sea: *Basin*
737 *Research*, v. 26, no. 4, p. 523-549.

738 White, N., 1990, Does the uniform stretching model work in the North Sea: *Tectonic evolution of the North Sea rifts*,
739 p. 217-240.

740 Wickham, J., and Moeckel, G., 1997, Restoration of structural cross-sections: *Journal of Structural Geology*, v. 19, no.
741 7, p. 975-986.

742 Wilson, P., Elliott, G. M., Gawthorpe, R. L., Jackson, C. A.-L., Michelsen, L., and Sharp, I. R., 2013, Geometry and
743 segmentation of an evaporite-detached normal fault array: 3D seismic analysis of the southern Bremstein
744 Fault Complex, offshore mid-Norway: *Journal of Structural Geology*, v. 51, p. 74-91.

745 Wilson, P., Elliott, G. M., Gawthorpe, R. L., Jackson, C. A., Michelsen, L., and Sharp, I. R., 2015, Lateral variation in
746 structural style along an evaporite-influenced rift fault system in the Halten Terrace, Norway: Influence of
747 basement structure and evaporite facies: *Journal of Structural Geology*, v. 79, p. 110-123.

748 Withjack, M. O., and Callaway, S., 2000, Active normal faulting beneath a salt layer: an experimental study of
749 deformation patterns in the cover sequence: *AAPG bulletin*, v. 84, no. 5, p. 627-651.

750 Withjack, M. O., Olson, J., and Peterson, E., 1990, Experimental models of extensional forced folds (1): *Aapg Bulletin*,
751 v. 74, no. 7, p. 1038-1054.

752 Ziegler, P., 1992, North Sea rift system: *Tectonophysics*, v. 208, no. 1, p. 55-75.

753

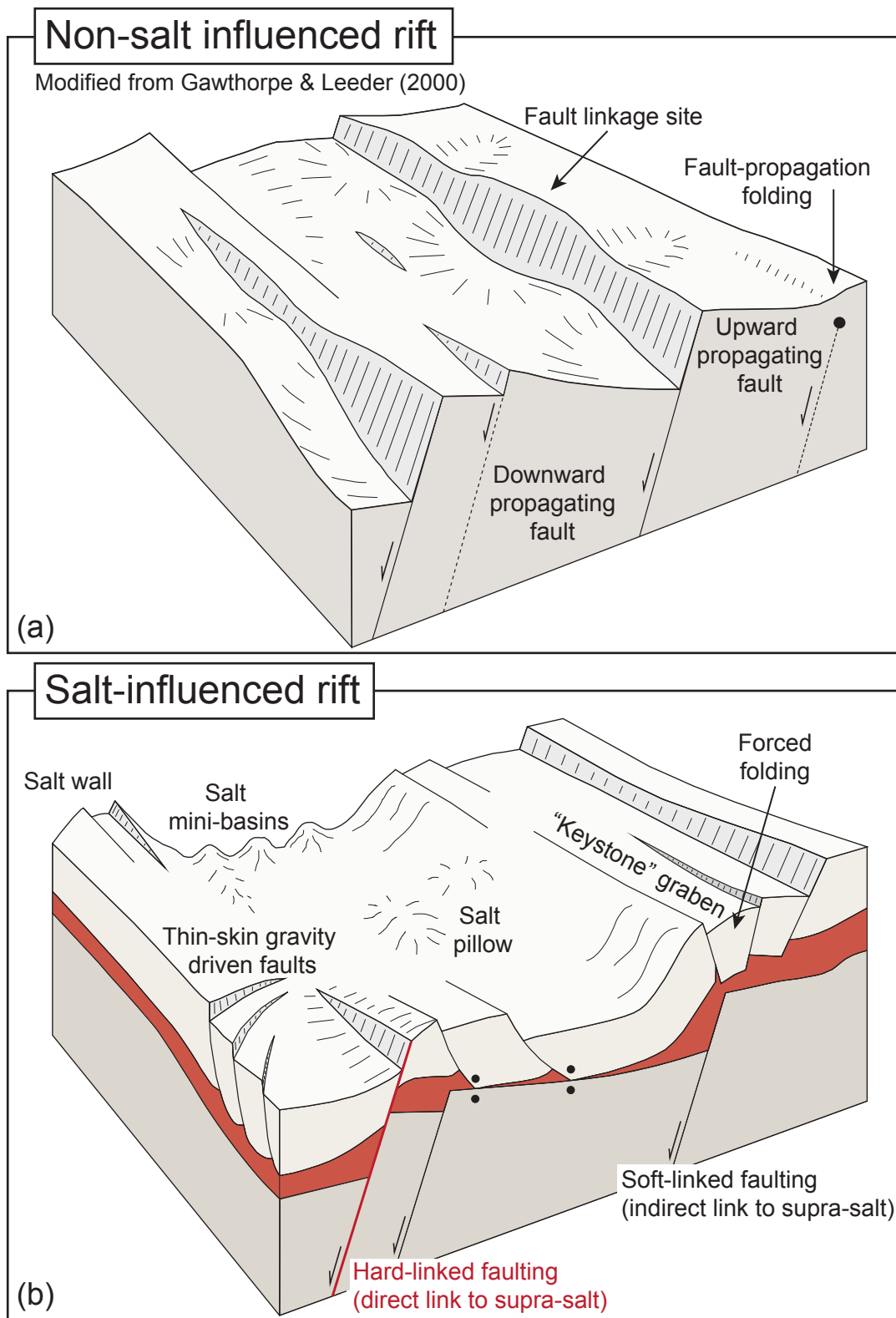
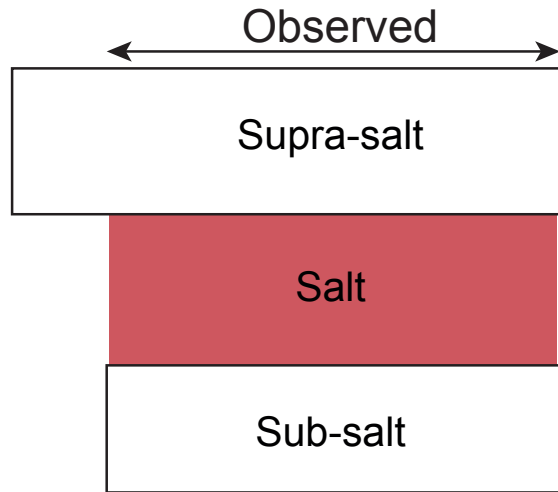
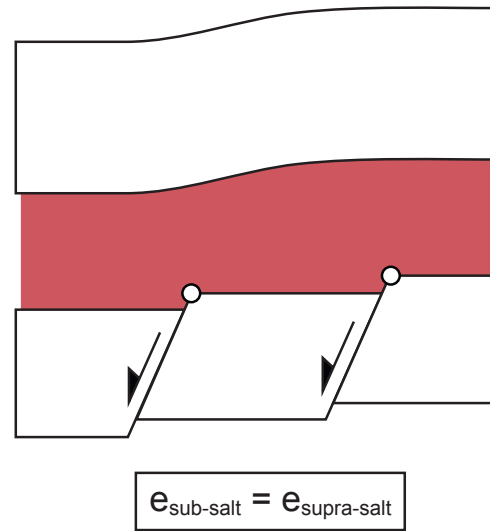


Figure 1 – Comparison of (a) non-salt influenced rifts (modified from Gawthorpe and Leeder, 2000), and (b) salt-influenced rift systems, documenting the large variation and increased complexity in structural style laterally and vertically associated with salt.

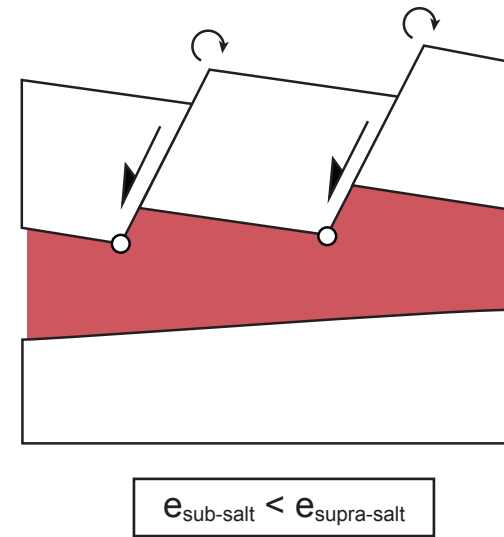
Initial system



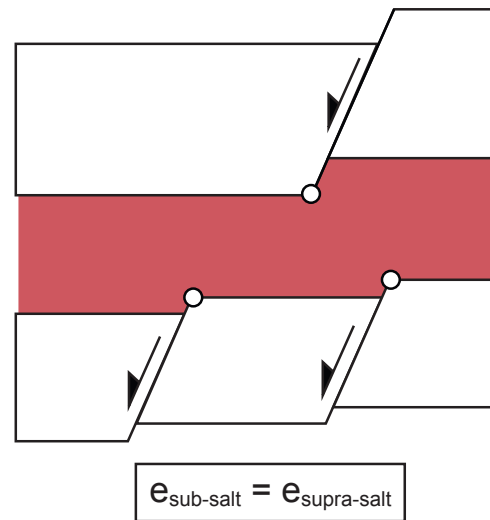
Balanced system



Unbalanced system



Balanced system



Unbalanced system

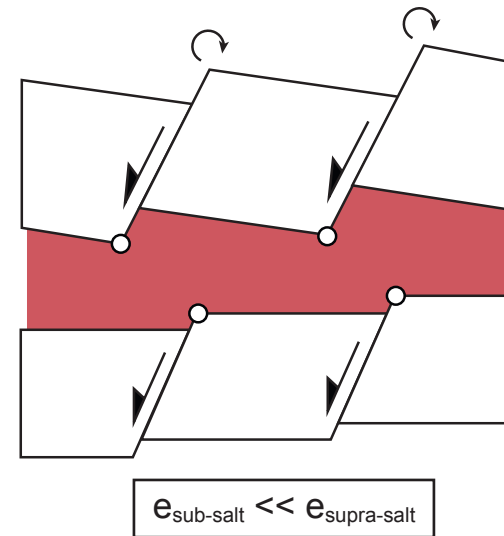


Figure 2 – End-member models documenting differing degrees of sub-salt and supra-salt extension. Balanced systems have undergone similar amounts of extension (e) at similar times (i.e. kinematically coherent), however, the supra- and sub- salt structural style may be largely different. In an unbalanced system supra- and sub- salt deformation is independent of one another.

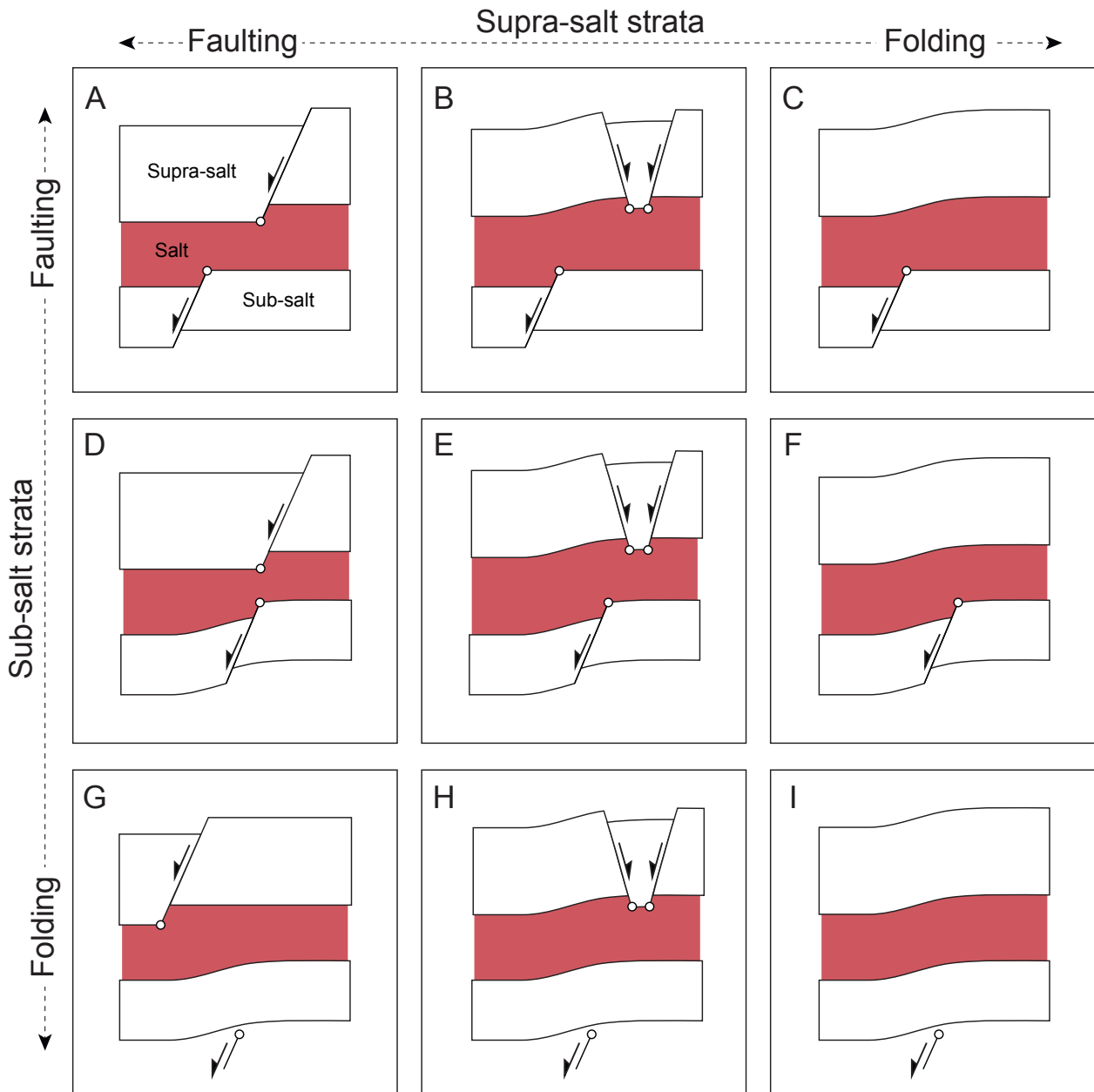


Figure 3 – Matrix documenting the sub- and supra- salt structure style variability, under similar amounts of extension (e). In all cases, the amount of extension in the sub-salt ($e_{\text{sub-salt}}$) and supra-salt ($e_{\text{supra-salt}}$) strata is the same.

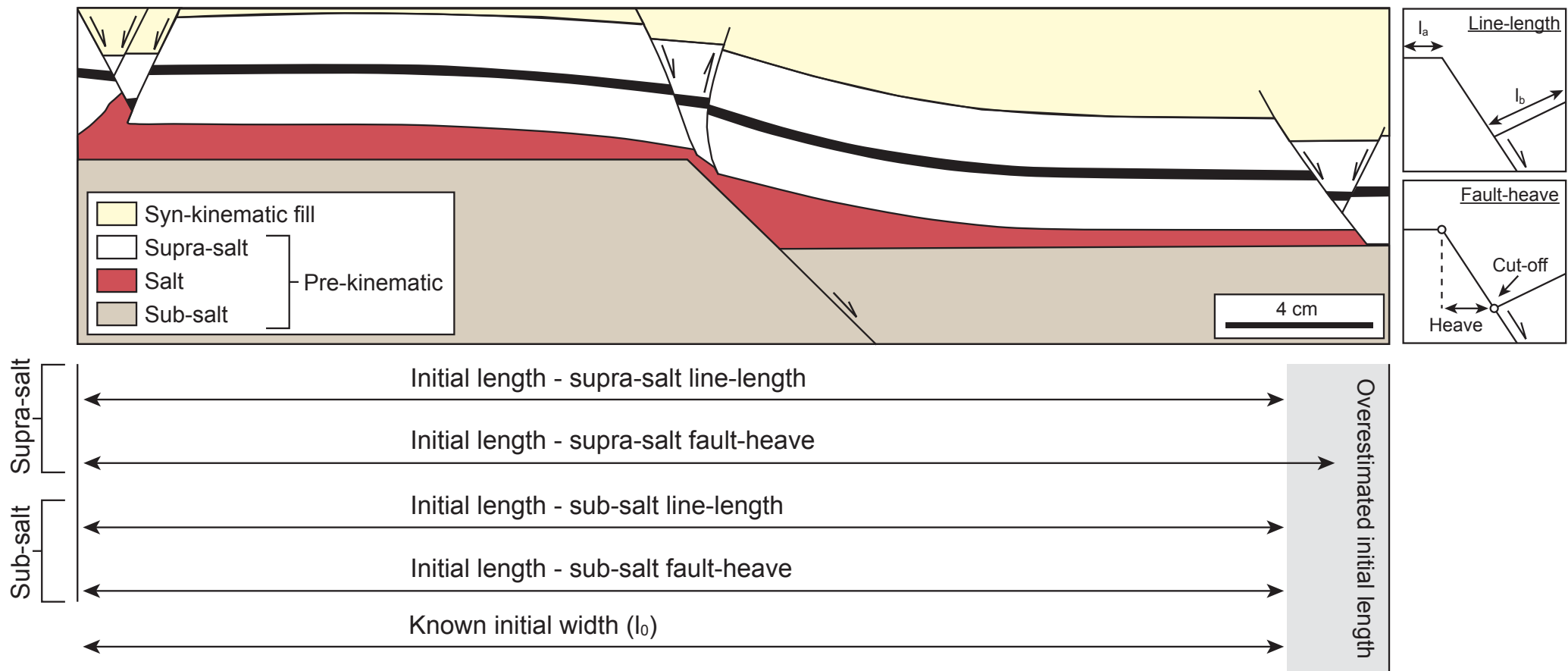


Figure 4 – A dry sand model of a forced fold (Model 7) from Withjack and Callaway (2000) overlying a sub-salt fault. The salt is shown in red, while the black horizon is a marker bed within the pre-kinematic supra-salt strata. The initial length (l_0) of the model is measured using a fault-heave summation and line-length approach, and compared to the known initial width to evaluate the accuracy of both methods. The sub-salt extension is comparable for fault-heave and line-length estimates, however, for the supra-salt, fault-heave predicts a greater initial width than line-length (shaded zone), and does not match the sub-salt. Vertical exaggeration is 1. Further details on the methodology are described in Appendix E.

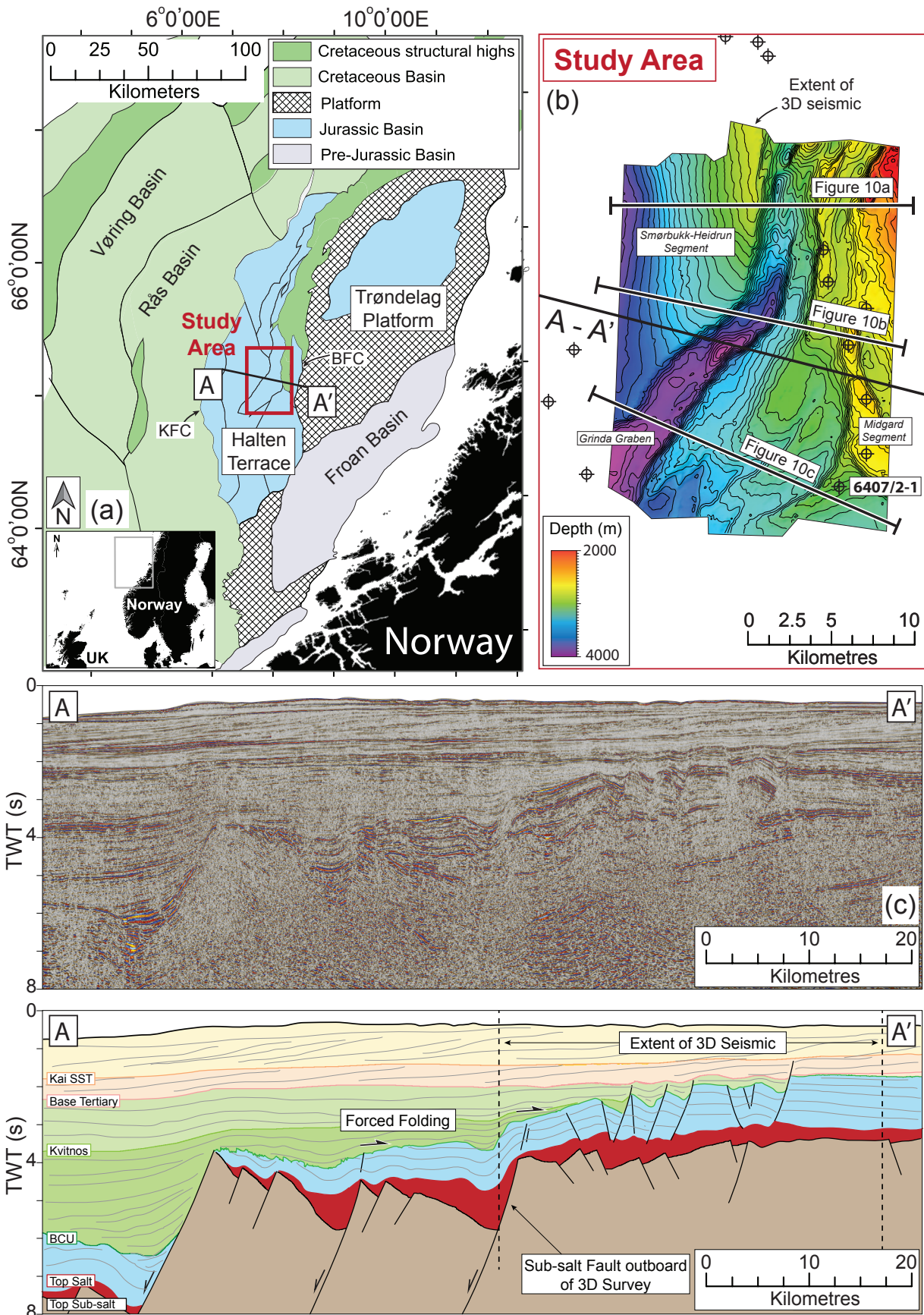


Figure 5 – (a) Major tectonic elements offshore Norway (modified from Elliott et al., 2012). The study area is shown in red. A regional section (A-A') is shown in black. KFC – Klakk Fault Complex, BFC – Bremstein Fault Complex. (b) BCU depth-structure map with 50 m contour intervals. Figure 10a-c seismic profiles are shown in black. Well 6407/2-1, used for the seismic-well tie in Appendix B, is also shown. (c) An uninterpreted and interpreted regional 2D seismic line through the Halten Terrace documenting the 3D seismic extent and regional structural style. See Figure 6 for the colours used in the seismic section. The 2D seismic line has not been used for calculating extension in Figure 7.

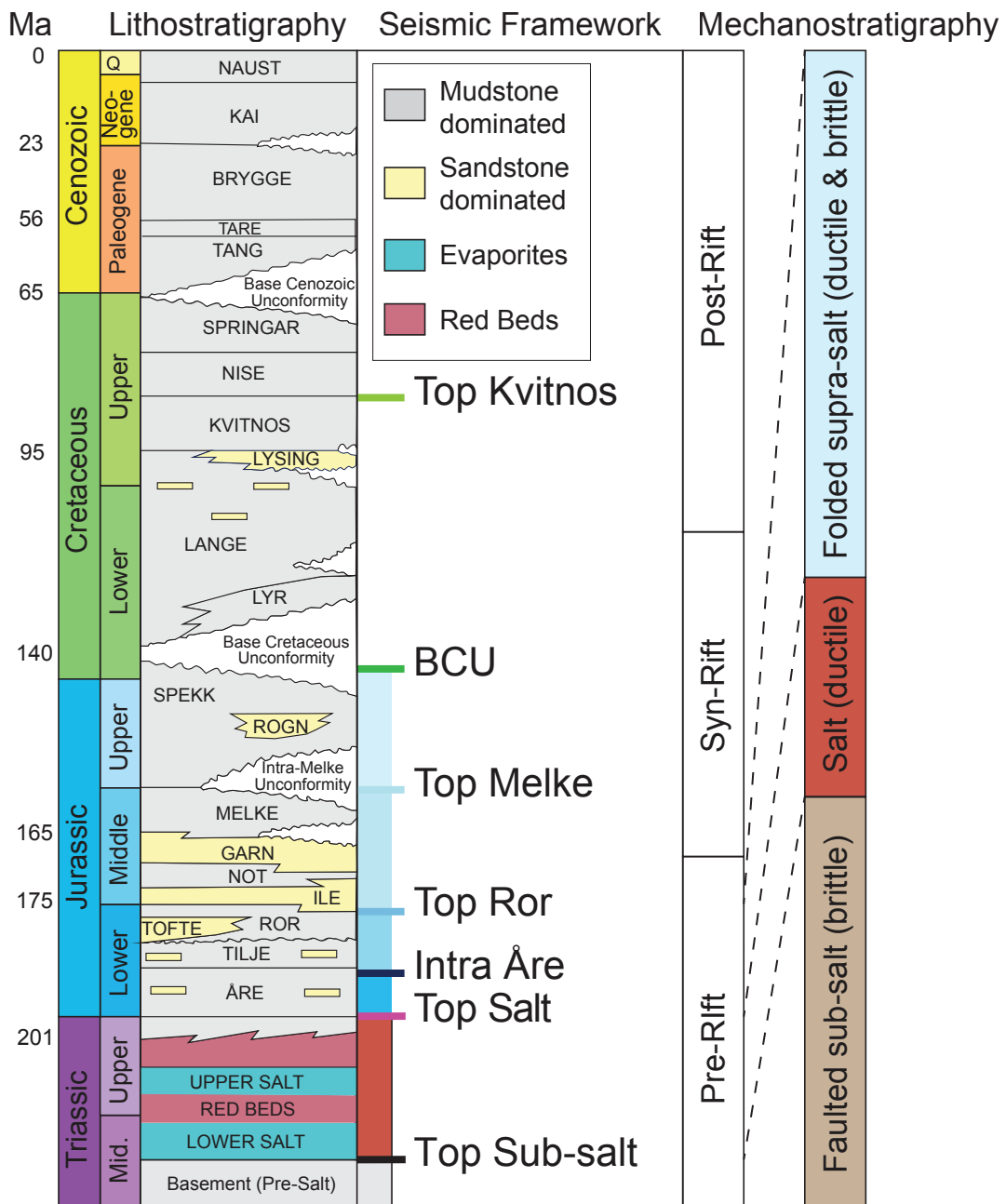


Figure 6 – Tectonostratigraphic chart for the Halten Terrace (modified from Marsh et al., 2010). Key interpreted seismic horizons discussed in this paper are shown, alongside the mechanostratigraphy. Colours representing the stratigraphy are used in Figure 5, 7 and 10.

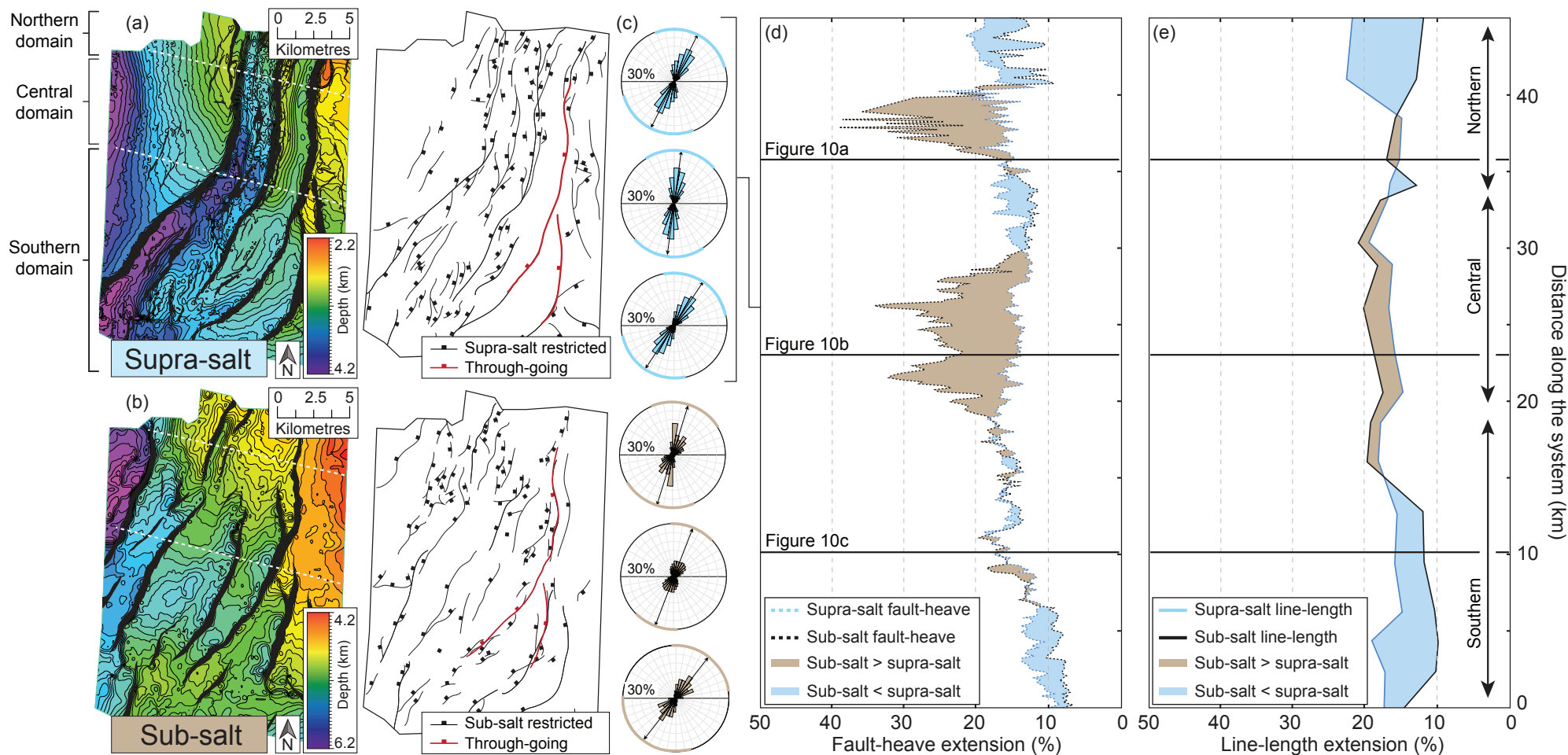


Figure 7 – Depth structure maps and interpreted fault traces for the (a) Top Ror – supra-salt, and (b) Top Sub-salt horizons. (c) Fault strike rose diagrams from north to south in the supra- and sub- salt strata. Black arrows and coloured circumference show the mean strike and circular variance, respectively. (d) Fault-heave and (e) line-length derived extension along the fault system. The approximate positions of the seismic sections in Figure 10 are also shown.

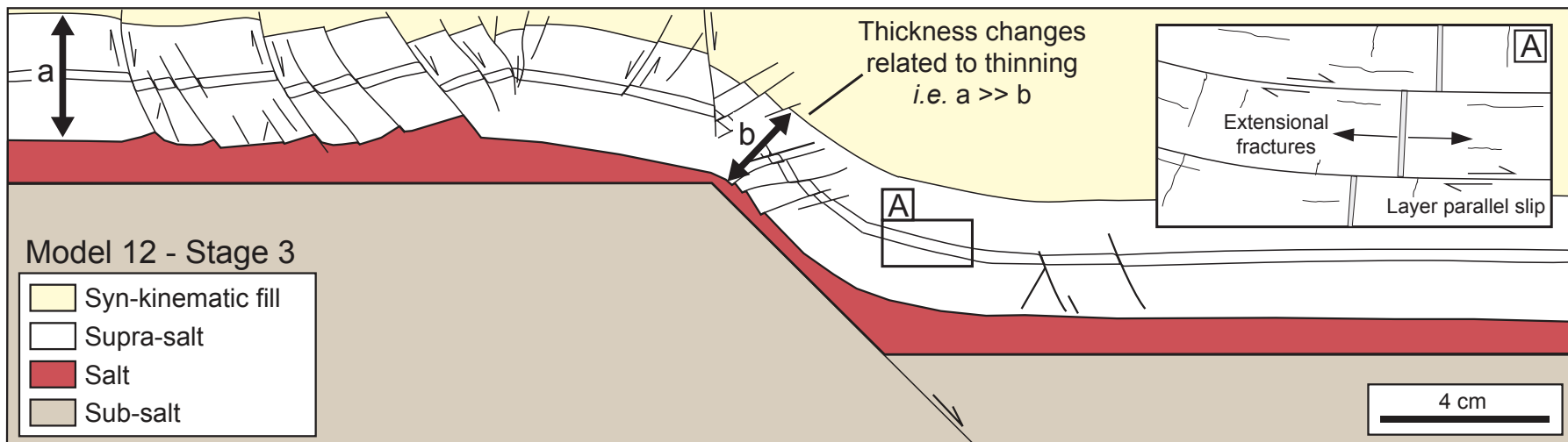


Figure 8 – Model 12 from Withjack and Callaway (2000) showing thickness changes related to stretching and a schematic of non-visible deformation ('diffuse deformation'). Vertical exaggeration is 1.

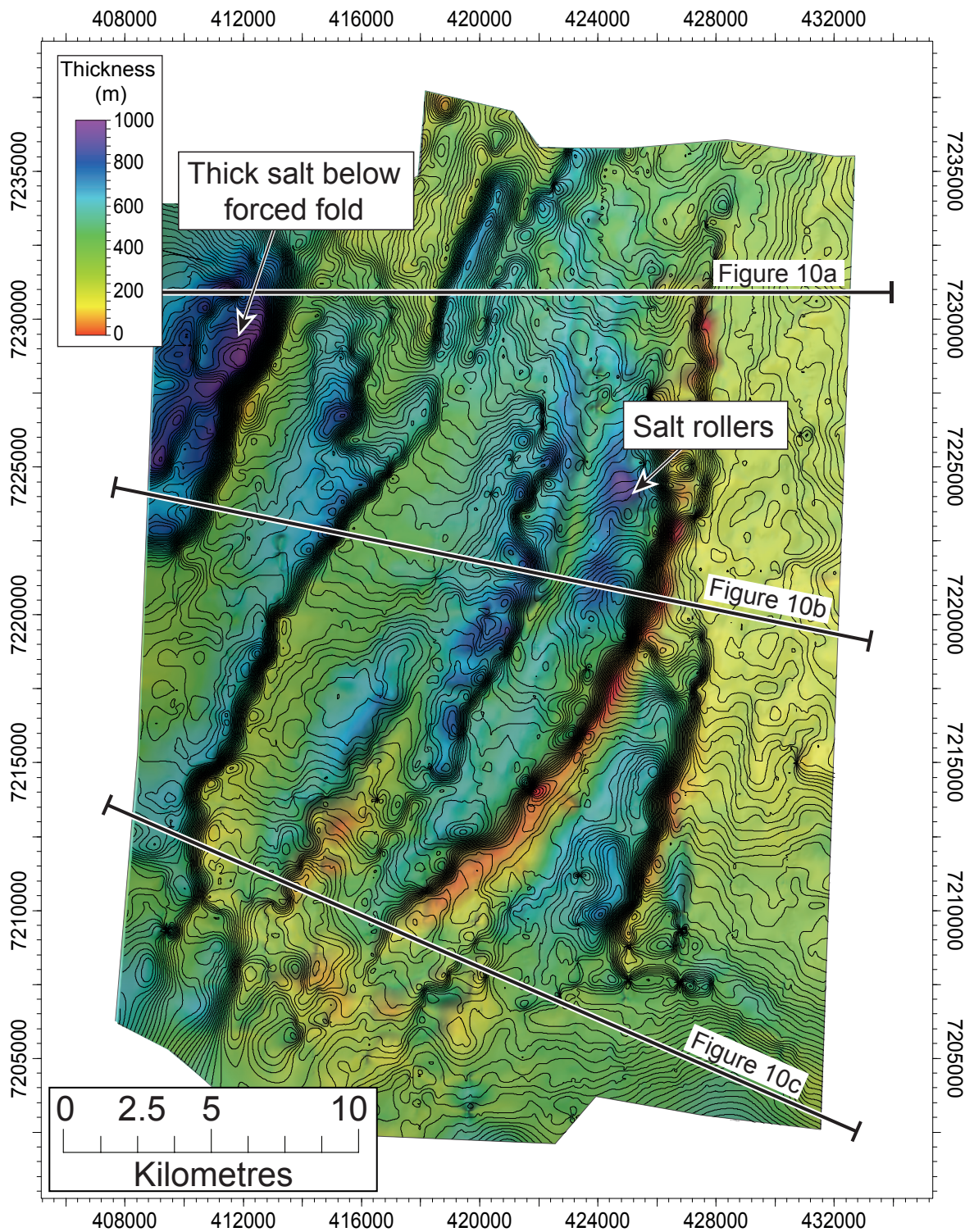


Figure 9 – Depth structure map for the Top Sub-salt horizon with a 50 m contour interval. The isochore (true vertical thickness) for the salt interval is overlain on the Top Sub-salt structure map as colours. Areas of purple represent thick salt, while red represents thin salt. The position of seismic sections in Figure 10 are also shown.

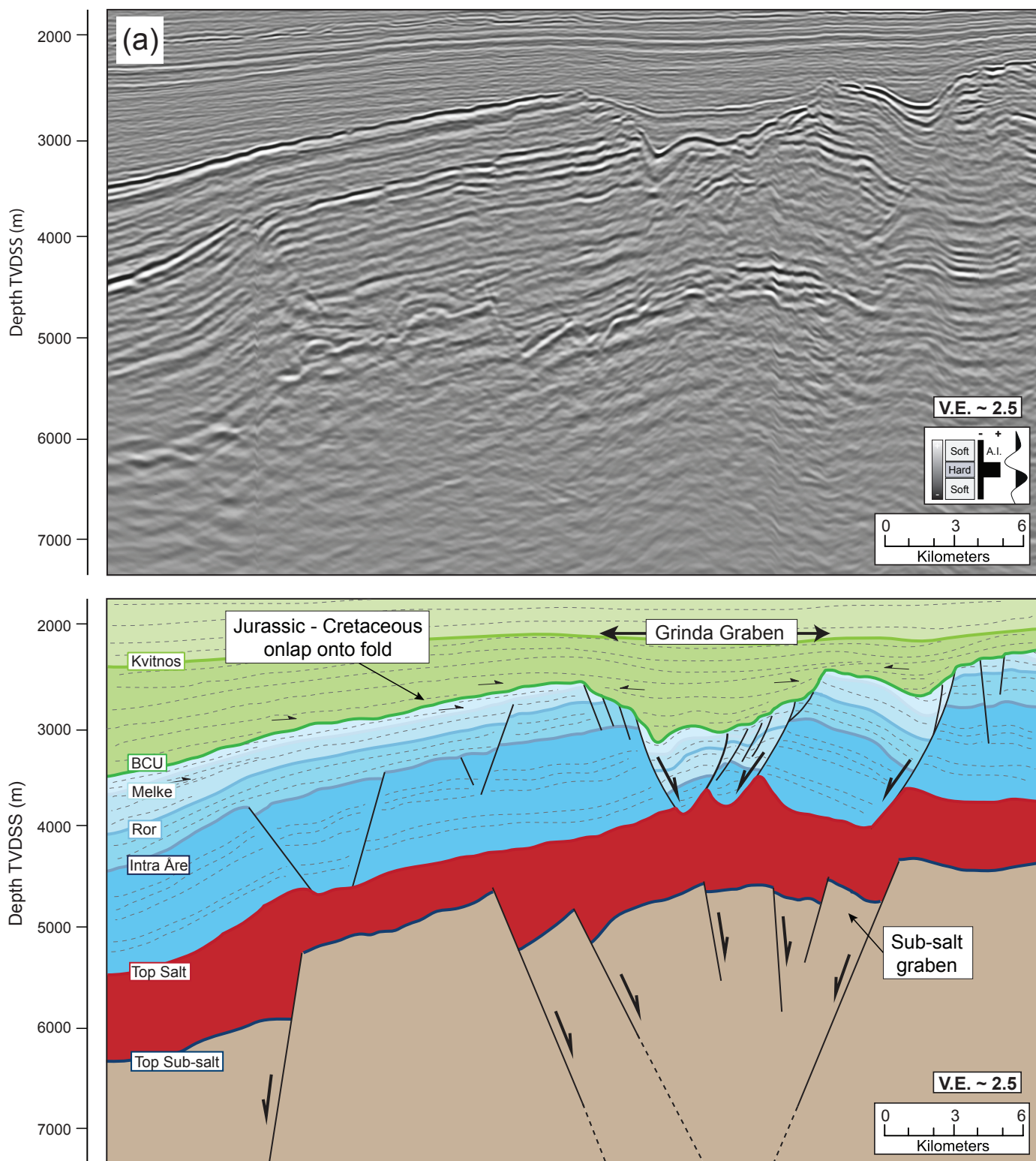


Figure 10 – Three uninterpreted (top) and interpreted (bottom) 2D seismic reflection profiles in the (a) north, (b) centre and (c) south of the 3D seismic volume. All sections have been depth converted using the time-depth relationship in Appendix C. The location of the sections is shown in Figure 5, and Figure 10. The colours on the interpreted sections are shown in Figure 6. Vertical exaggeration is 2.5. These sections have been used to document the structural style and were not used to calculate extension in Figure 7.

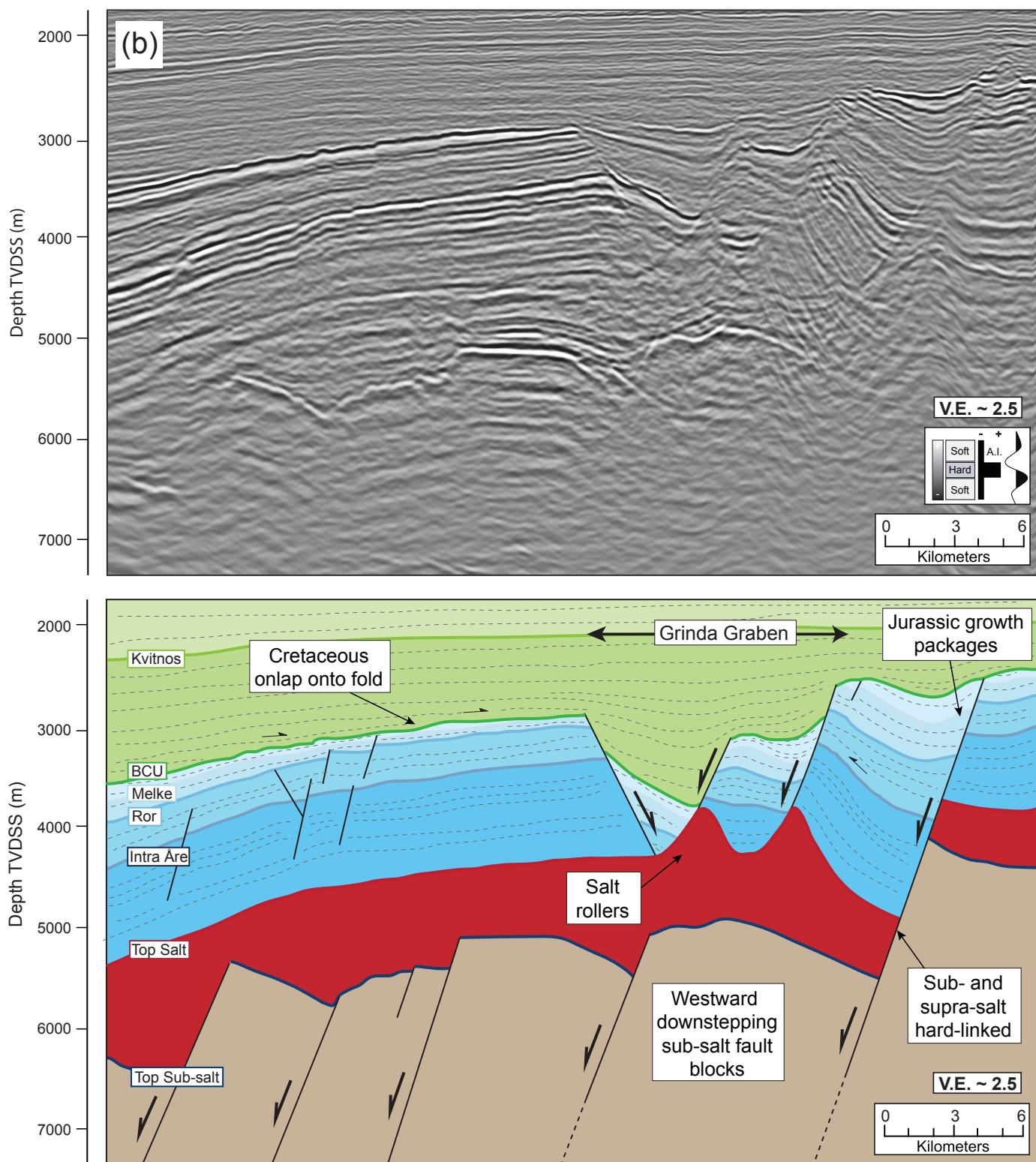


Figure 10 – Three uninterpreted (top) and interpreted (bottom) 2D seismic reflection profiles in the (a) north, (b) centre and (c) south of the 3D seismic volume. All sections have been depth converted using the time-depth relationship in Appendix C. The location of the sections is shown in Figure 5, and Figure 10. The colours on the interpreted sections are shown in Figure 6. Vertical exaggeration is 2.5. These sections have been used to document the structural style and were not used to calculate extension in Figure 7.

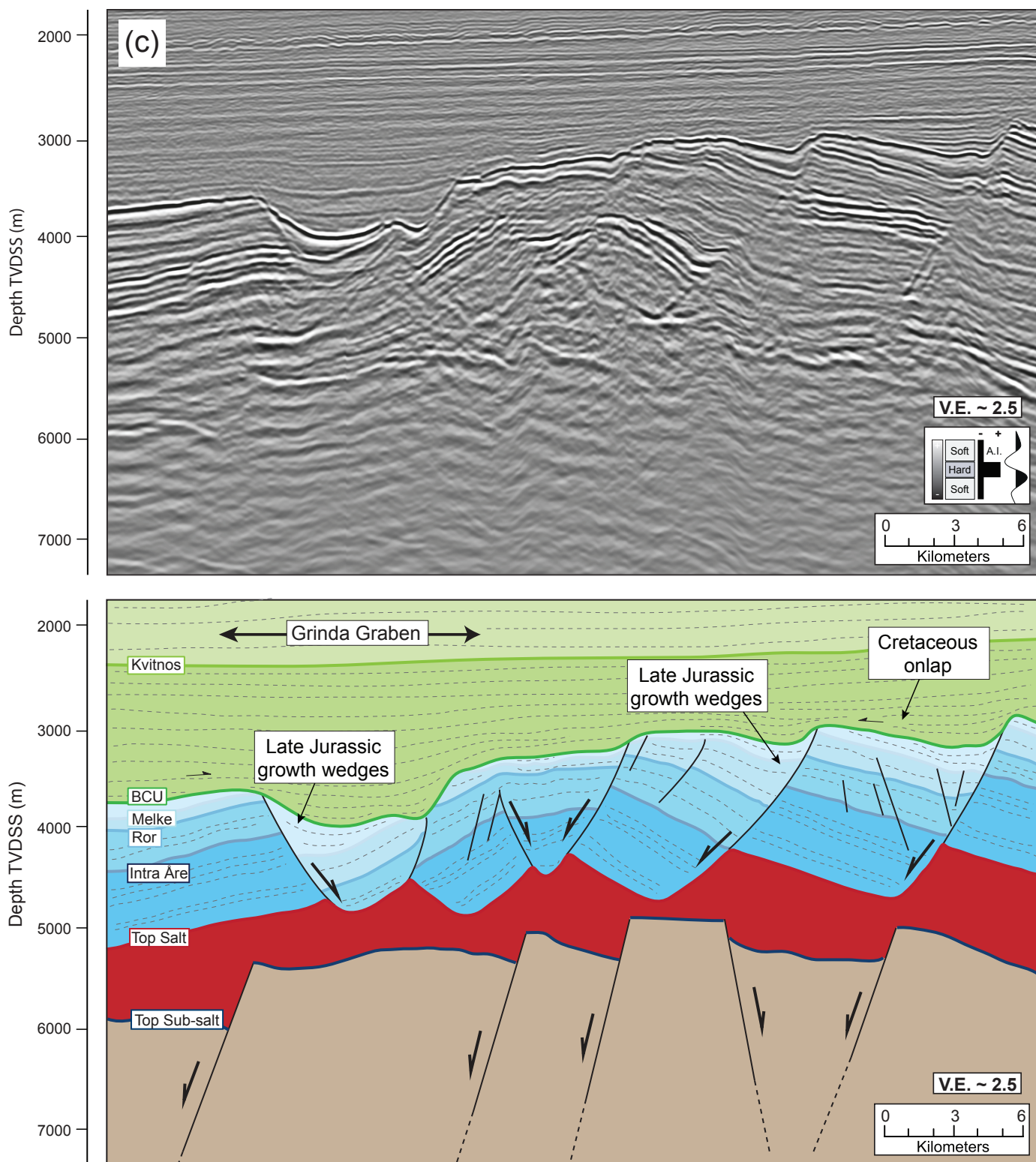


Figure 10 – Three uninterpreted (top) and interpreted (bottom) 2D seismic reflection profiles in the (a) north, (b) centre and (c) south of the 3D seismic volume. All sections have been depth converted using the time-depth relationship in Appendix C. The location of the sections is shown in Figure 5, and Figure 10. The colours on the interpreted sections are shown in Figure 6. Vertical exaggeration is 2.5. These sections have been used to document the structural style and were not used to calculate extension in Figure 7.

Term	Definition
Ductile strain	A change in shape produced by structures which are too small to be imaged individually by a particular technique and/or too small to be represented individually on a given cross-section or map, albeit in a physical model or seismic data (Walsh and Watterson, 1996).
Brittle strain	Discontinuities that can be imaged by a particular technique on a given cross-section or map e.g. a fault, albeit in a physical model or seismic (Walsh and Watterson, 1996).
Thin-skinned	Deformation that is restricted to the detachment and its overburden. It is typically driven by gravity (e.g. Brun and Fort, 2011), although it may occur during stretching of the entire crust or rifting (see ‘thick-skinned’).
Thick-skinned	Deformation involving sub- and supra-salt stratigraphy, and the salt layer itself, driven by whole-plate stretching or rifting .
Supra-salt	Rock units overlying and deformation occurring above the salt. Synonymous with the terms ‘cover’ and ‘overburden’.
Sub-salt	Rock units underlying and deformation occurring below the salt. Synonymous with ‘acoustic basement’.
Decoupling	Sub- and supra-salt strata deform differently producing a variety of structural styles (e.g. Withjack et al., 1990; Jarrige, 1992).
Kinematic coherence	The timing and rates of displacement at each point on all faults in an array are largely synchronous. Not all points on all fault surfaces will be active throughout the life of the array, but the time of fault initiation and death, and growth rate, are fixed in relation to the overall growth history of the array (Walsh and Watterson, 1991). Individual faults within the array need not be physically connected.
Geometric coherence	Displacements on faults may aggregate to produce a displacement distribution resembling a single fault (Walsh and Watterson, 1991; Childs et al., 1995).
Soft-linked fault(s)	Faults surfaces which, at the scale of observation, appear physically disconnected, but between which mechanical and geometrical continuity is achieved by ductile strain in the intervening rock volume (Walsh and Watterson, 1991).
Hard-linked fault(s)	Fault surfaces that are, at the scale of observation, physically connected (Walsh and Watterson, 1991).

Table 1 – Summary of fault nomenclature used in this study.

Model name	Supra-salt strata	Initial supra-salt thickness (mm)	Initial salt thickness (mm)	Initial length, l_0 (mm)	Final length, l_1 (mm)
Model 7	Dry sand	10.0	30.0	330.0	360.0
Model 8	Dry sand	10.0	30.0	330.0	360.0
Model 9	Dry sand	10.0	30.0	330.0	360.0
Model 12	Wet clay	10.0	30.0	330.0	360.0

Table 2 – Description of models from Withjack and Callaway (2000). All models are shown in Appendix A.

Model name	Restoration method	Extension, e (mm)	Extension, E (%)	Sub- or supra- salt
7 – Stage 1	Fault-heave	1.0	0.3	Supra-salt
7 – Stage 2	Fault-heave	3.0	0.8	Supra-salt
7 – Stage 3	Fault-heave	12.0	3.3	Supra-salt
7 – Stage 1	Fault-heave	4.0	1.2	Sub-salt
7 – Stage 2	Fault-heave	18.0	5.3	Sub-salt
7 – Stage 3	Fault-heave	34.0	9.9	Sub-salt
7 – Stage 1	Line-length	3.0	0.9	Supra-salt
7 – Stage 2	Line-length	20.0	5.9	Supra-salt
7 – Stage 3	Line-length	34.0	9.9	Supra-salt
7 – Stage 1	Line-length	4.0	1.2	Sub-salt
7 – Stage 2	Line-length	18.0	5.3	Sub-salt
7 – Stage 3	Line-length	34.0	9.9	Sub-salt
7 – Stage 1		3.8	1.2	Both
7 – Stage 2	Known values	17.2	5.2	Both
7 – Stage 3		29.7	9.0	Both

Table 3 – A comparison of measured extension using the line-length and fault-heave methods with the known values for Model 7 from Withjack and Callaway (2000). The amount of extension (e) is the difference between the final and initial length of the model ($e = l_1 - l_0$). The percentage of extension (E) is the ratio of the amount of extension to the initial length ($E = e/l_0$).

Model name	Restoration method	Extension, e (mm)	Extension, E (%)	Sub- or supra- salt
8 – Stage 1	Fault-heave	3.0	0.9	Supra-salt
8 – Stage 2	Fault-heave	2.0	0.5	Supra-salt
8 – Stage 3	Fault-heave	6.0	1.6	Supra-salt
8 – Stage 1	Fault-heave	1.0	0.3	Sub-salt
8 – Stage 2	Fault-heave	19.0	5.5	Sub-salt
8 – Stage 3	Fault-heave	31.0	9.0	Sub-salt
8 – Stage 1	Line-length	5.0	1.5	Supra-salt
8 – Stage 2	Line-length	18.0	5.2	Supra-salt
8 – Stage 3	Line-length	31.0	9.0	Supra-salt
8 – Stage 1	Line-length	1.0	0.3	Sub-salt
8 – Stage 2	Line-length	19.0	5.5	Sub-salt
8 – Stage 3	Line-length	31.0	9.0	Sub-salt
8 – Stage 1		6.7	2.0	Both
8 – Stage 2	Known values	20.7	6.3	Both
8 – Stage 3		29.7	9.0	Both

Table 4 – A comparison of measured extension using the line-length and fault-heave methods with the known values for Model 8 from Withjack and Callaway (2000). The amount of extension (e) is the difference between the final and initial length of the model ($e = l_1 - l_0$). The percentage of extension (E) is the ratio of the amount of extension to the initial length ($E = e/l_0$).

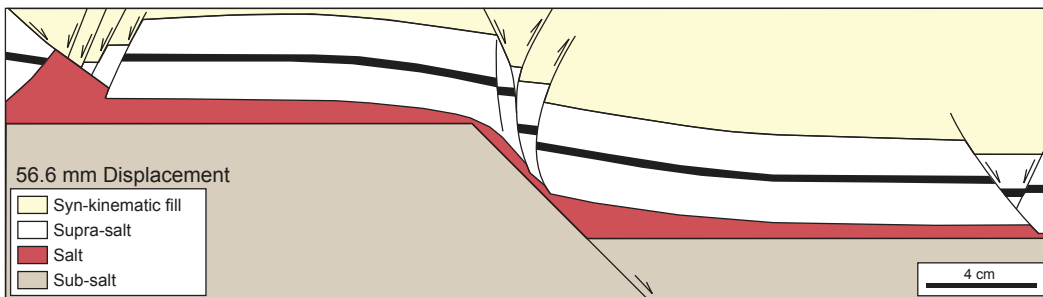
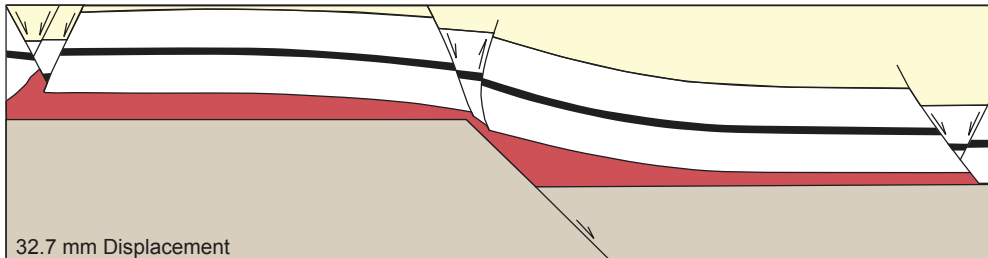
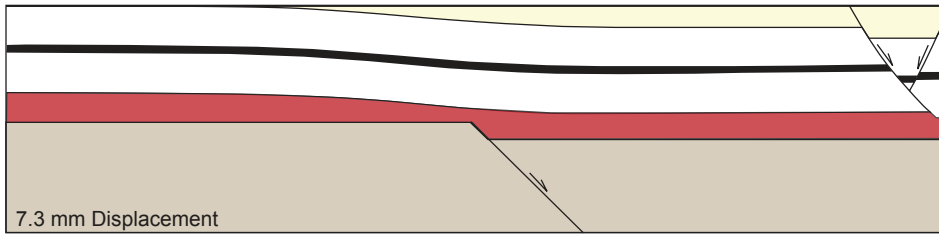
Model name	Restoration method	Extension, e (mm)	Extension, E (%)	Sub- or supra- salt
9 – Stage 1	Fault-heave	10.0	2.9	Supra-salt
9 – Stage 2	Fault-heave	18.0	5.3	Supra-salt
9 – Stage 3	Fault-heave	36.0	10.6	Supra-salt
9 – Stage 1	Fault-heave	11.0	3.3	Sub-salt
9 – Stage 2	Fault-heave	17.0	5.0	Sub-salt
9 – Stage 3	Fault-heave	35.0	10.3	Sub-salt
9 – Stage 1	Line-length	10.0	2.9	Supra-salt
9 – Stage 2	Line-length	19.0	5.6	Supra-salt
9 – Stage 3	Line-length	36.0	10.6	Supra-salt
9 – Stage 1	Line-length	11.0	3.3	Sub-salt
9 – Stage 2	Line-length	17.0	5.0	Sub-salt
9 – Stage 3	Line-length	35.0	10.3	Sub-salt
9 – Stage 1		8.7	2.6	Both
9 – Stage 2	Known values	14.3	4.3	Both
9 – Stage 3		29.7	9.0	Both

Table 5 – A comparison of measured extension using the line-length and fault-heave methods with the known values for Model 9 from Withjack and Callaway (2000). The amount of extension (e) is the difference between the final and initial length of the model ($e = l_1 - l_0$). The percentage of extension (E) is the ratio of the amount of extension to the initial length ($E = e/l_0$).

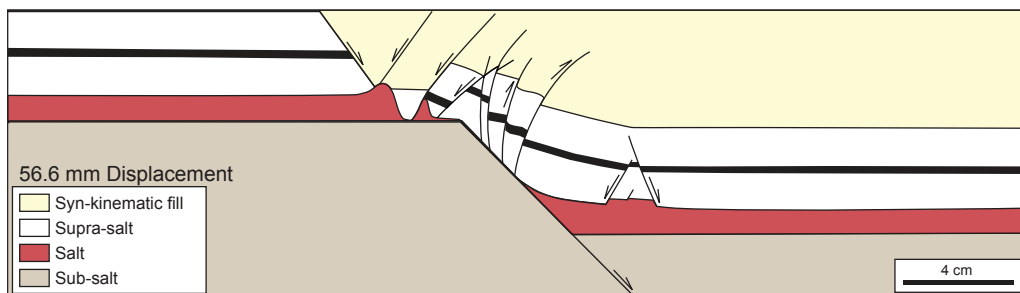
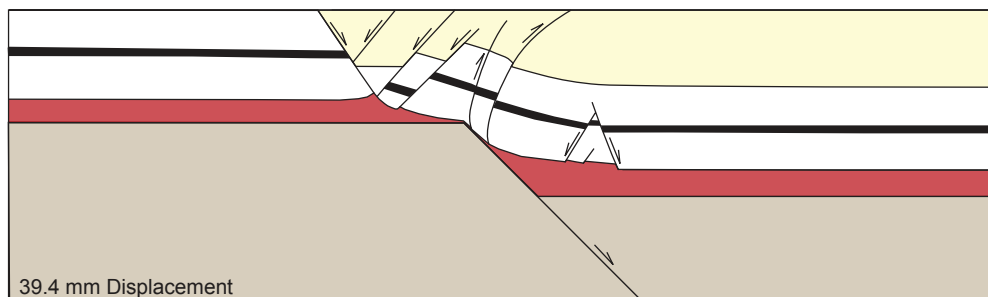
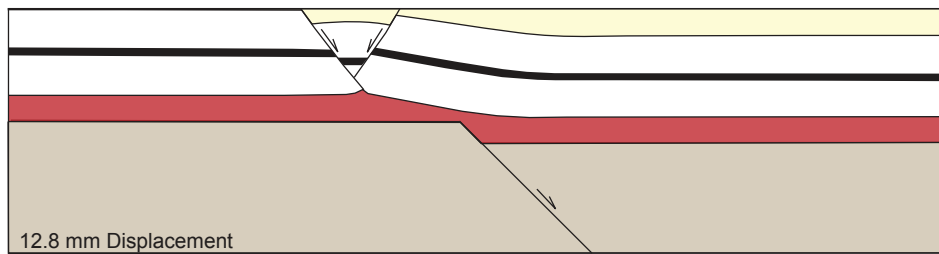
Model name	Restoration method	Extension, e (mm)	Extension, E (%)	Sub- or supra- salt
12 – Stage 1	Fault-heave	11.0	3.1	Supra-salt
12 – Stage 2	Fault-heave	18.0	5.1	Supra-salt
12 – Stage 3	Fault-heave	24.0	6.8	Supra-salt
12 – Stage 1	Fault-heave	20.0	5.8	Sub-salt
12 – Stage 2	Fault-heave	26.0	7.6	Sub-salt
12 – Stage 3	Fault-heave	33.0	9.6	Sub-salt
12 – Stage 1	Line-length	5.0	1.4	Supra-salt
12 – Stage 2	Line-length	3.0	0.8	Supra-salt
12 – Stage 3	Line-length	8.0	2.2	Supra-salt
12 – Stage 1	Line-length	20.0	5.8	Sub-salt
12 – Stage 2	Line-length	26.0	7.6	Sub-salt
12 – Stage 3	Line-length	33.0	9.6	Sub-salt
12 – Stage 1		18.8	5.7	Both
12 – Stage 2	Known values	24.5	7.4	Both
12 – Stage 3		29.7	9.0	Both

Table 6 – A comparison of measured extension using the line-length and fault-heave methods with the known values for Model 12 from Withjack and Callaway (2000). The amount of extension (e) is the difference between the final and initial length of the model ($e = l_1 - l_0$). The percentage of extension (E) is the ratio of the amount of extension to the initial length ($E = e/l_0$).

Model 7

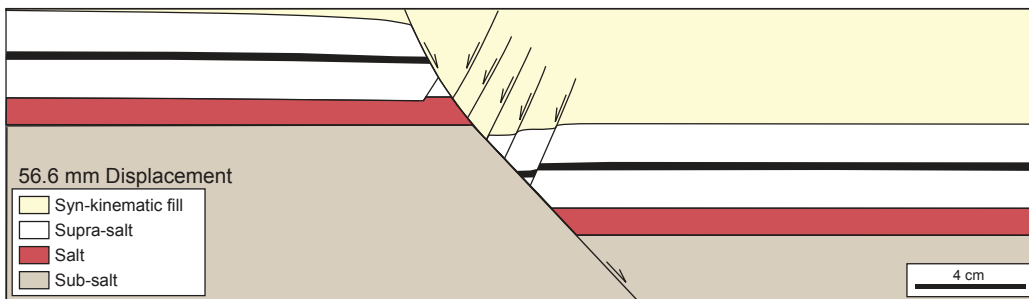
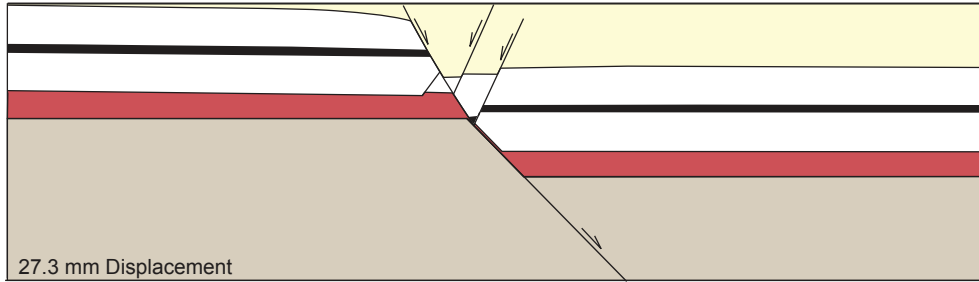
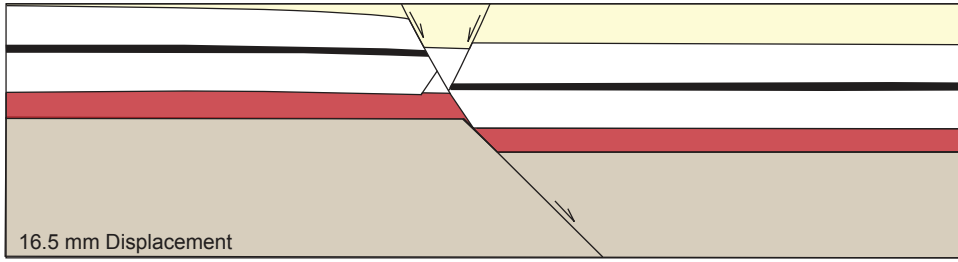


Model 8

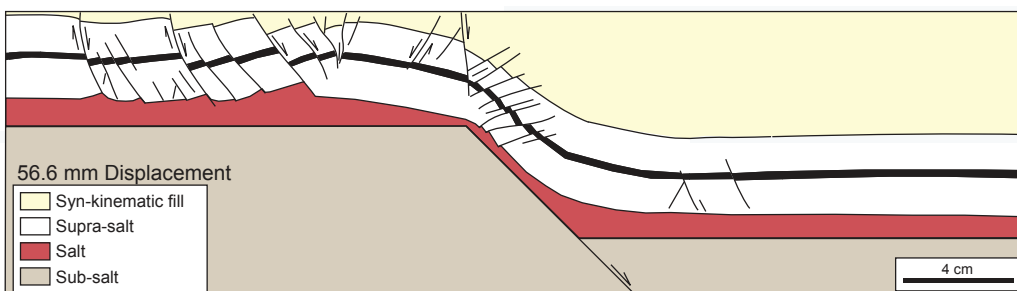
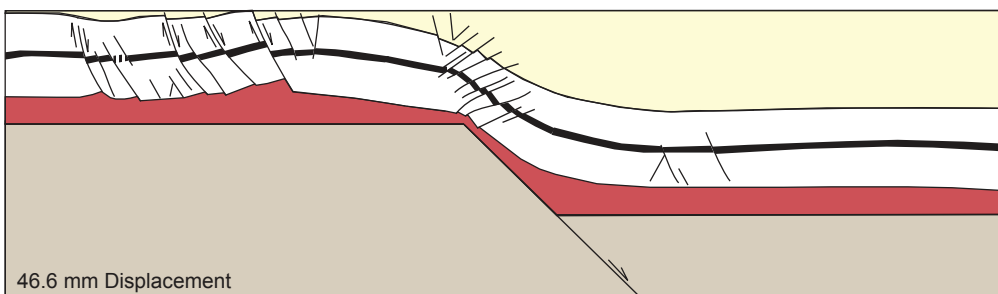
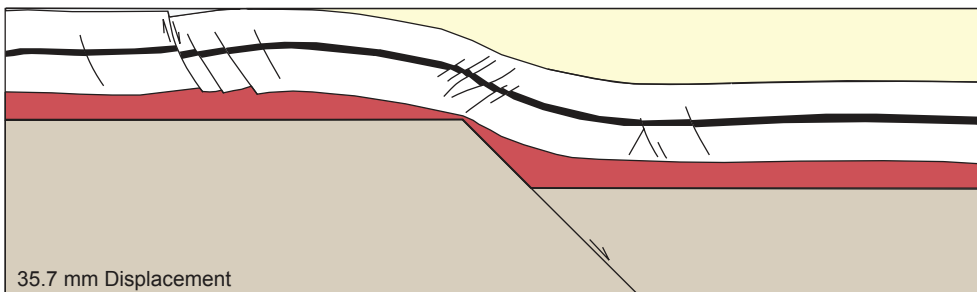


Appendix A – Models 7 and 8 from Withjack and Callaway (2000). Vertical exaggeration is 1.

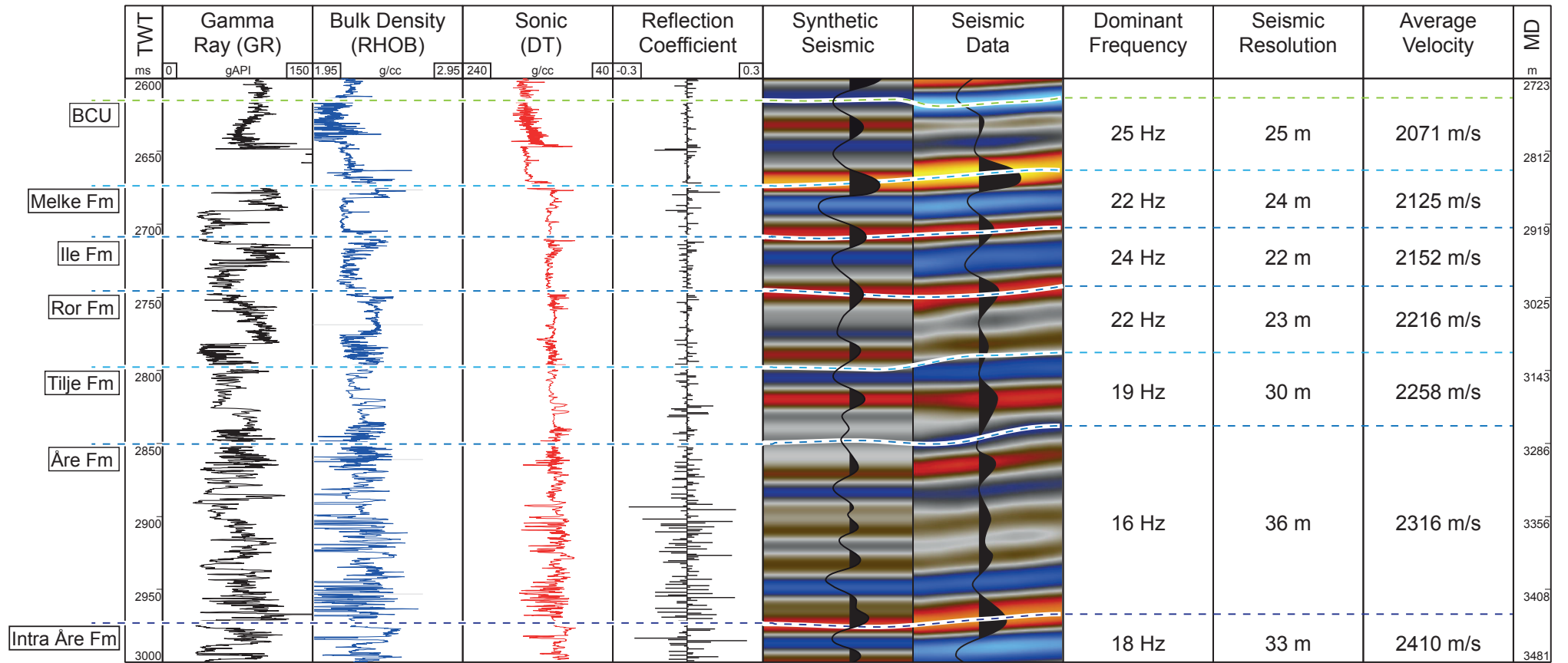
Model 9



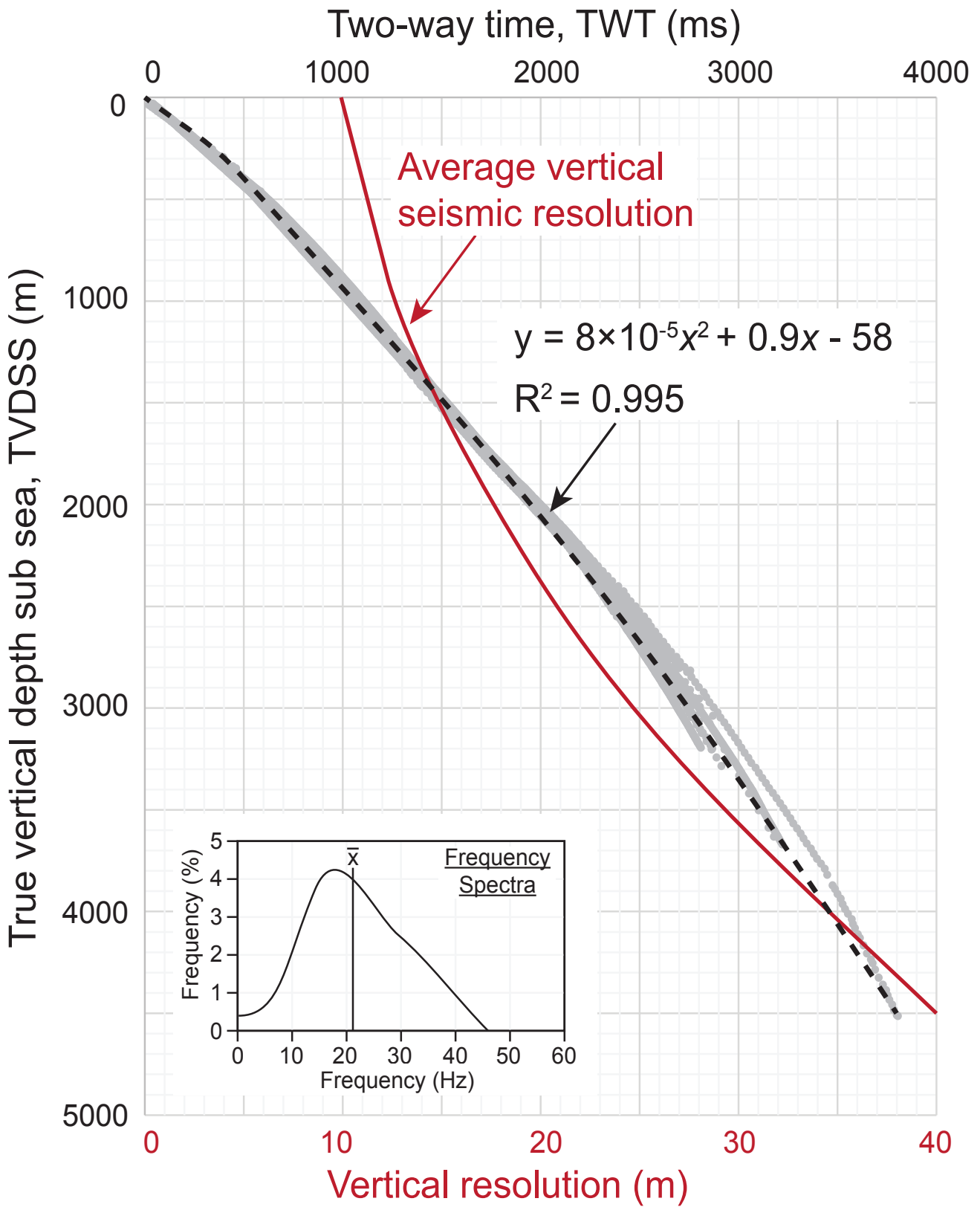
Model 12



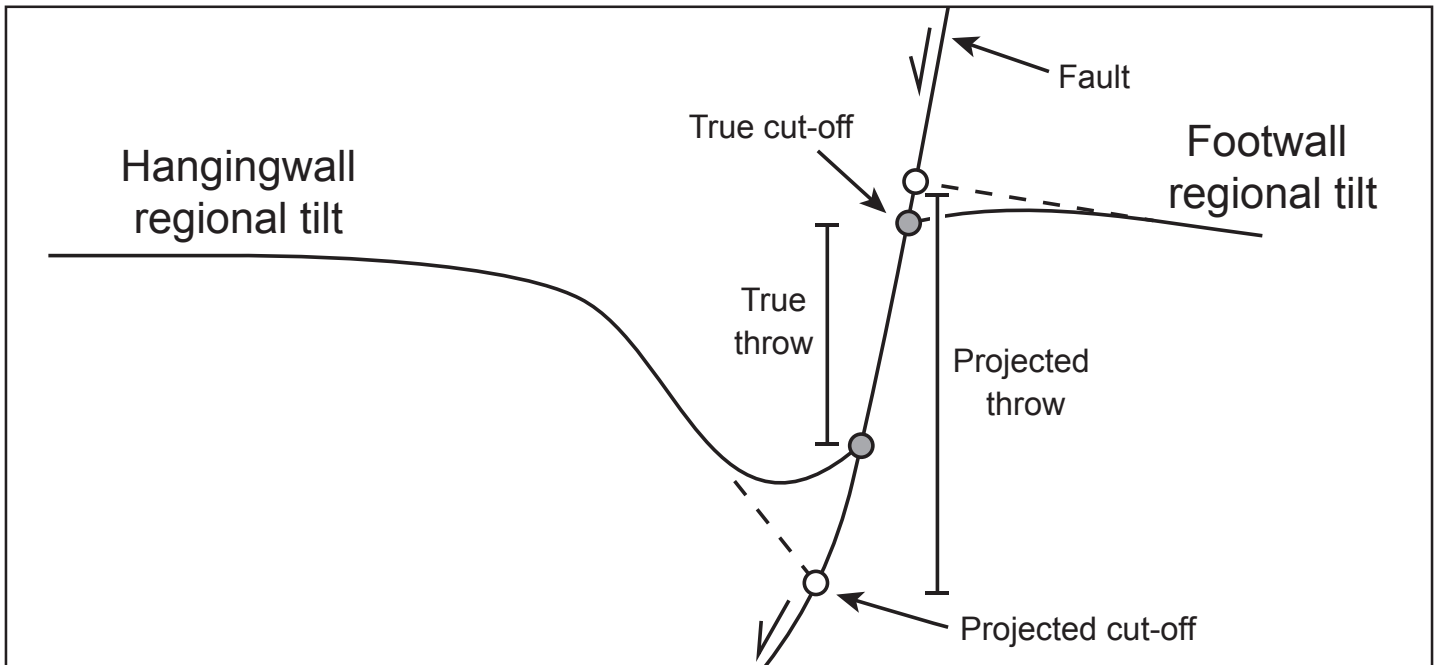
Appendix A continued – Models 9 and 12 from Withjack and Callaway (2000). Vertical exaggeration is 1.



Appendix B – Synthetic seismogram generated for well 6407/2-1 showing the correlation of the Jurassic and Cretaceous stratigraphy to the seismic section. The measured average velocity and the average seismic frequency for each interval are shown and used to calculate vertical resolution with depth. See Figure 5 for the well location. Some horizons have been omitted from the main text and figures 5 and 10 due to the close vertical spacing between the Jurassic strata, see Appendix E for further details.



Appendix C – Time-depth relationship (black dashed line) derived from Halten Terrace checkshots (grey circles). The average vertical seismic resolution (red solid line) was calculated using the frequency and velocity.



Appendix D – Schematic diagram illustrating the projection of hangingwall and footwall cut-offs in section.

Appendix E

1. Halten Terrace detailed methods

1.1 Seismic dataset

The 3D seismic survey covers an area of c. 3250 km² of the Halten Terrace, offshore Norway. The dataset is time-migrated, zero phase and European Polarity (Brown, 2001), with a vertical sampling rate of 4 ms TWT and a record length of 6000 ms. Inline and crossline spacing is 12.5m. Vertical resolution ranges from c. 13m at <1 km utilising a central frequency of c. 40 Hz with a velocity of c. 2000 ms⁻¹, to c. 67 m utilising a central frequency of c. 20 Hz with a velocity of c. 4000 ms⁻¹ at 4km (Appendix B - C).

1.2 Horizon mapping

8 wells, containing a suite of wireline logs, checkshots and core-constrained formation tops, were tied to the seismic data to constrain 13 seismic surfaces, two within the Triassic interval, six within the Jurassic and five in the Cretaceous – Tertiary intervals. Given the close vertical spacing between Jurassic horizons (Appendix B) and our focus on the Triassic – Early Cretaceous interval, not all horizons are shown in the main text or in the restoration (Appendix F). None of the wells penetrated below the uppermost Triassic, hence seismic facies analysis was used to interpret the Top Salt and Top Sub-salt (i.e. Base Salt), similar to prior studies (Marsh et al., 2010; Richardson et al., 2005; Stewart et al., 1996). The salt is typically chaotic, of low amplitude, and primarily discontinuous, except at its top and base. Parallel, continuous reflections with moderate-high amplitudes characterise the strata above the salt. We refer to the units above the salt as ‘supra-salt’.

1.3 Fault mapping

Faults, tiplines and branchlines were mapped across the seismic volume using breaks and displacement in seismic reflections. Each fault segment was categorised into those that are restricted to the (i) supra-salt and (ii) sub-salt intervals, and those involving (iii) sub- and supra-salt stratigraphy. The study area was then divided into three domains based upon the dominant fault strike in the supra-salt strata: (i) northern – NE-SW striking (Fig. 10a), (ii) central – N-S striking (Fig. 10b), and (iii) southern – NE-SW striking (Fig. 10c).

1.4 Depth conversion

Velocities for the depth conversion are derived from checkshot data from 8 wells throughout the eastern Halten Terrace (Appendix C). Checkshots covered a depth range from near the sea bed to the uppermost Triassic. No wells penetrated into salt, so a velocity of 4000 ms⁻¹ was assumed, which is less than typical velocities used for halite (4500 ms⁻¹), as mud interbeds are common (Wilson et al., 2013; Wilson et al., 2015). The sub-salt strata were also assumed to be 4000 ms⁻¹. The velocities used for depth conversion (Appendix B-C) are similar to those derived potential field modelling and refraction data (Breivik et al., 2009; Breivik et al., 2011), and well-derived velocity studies (Storvoll et al., 2005). Errors associated with the velocity errors are discussed in sections 2.2. and 2.3.

2. Measuring extension in sections

2.1 Fault-heave summation

Horizontal extension (e) was calculated for two pre-kinematic horizons, one above and one below the salt. Fault heave was measured perpendicular to the dominant fault strike, and summed to give a total fault heave along the horizon of interest between horizon cut-offs. Cut-offs were defined using an extrapolated line that follows the regional trend of the chosen horizon prior to folding (Appendix D) (Wilson et al., 2013), removing the effect of fault-parallel folding (Walsh et al., 1996). By measuring the present-day width of the section (l_1), the pre-extension initial width can be calculated ($l_0 = l_1 - e$). The percentage of extension of the pre-extension width (E) was calculated using a ratio of total fault heave (horizontal extension, e) to the pre-extension width i.e. $E = e / l_0$. This method only considers brittle deformation, and does not require a velocity model as all deformation is assumed to be horizontal. However, when projecting the horizon cut-offs, velocity models will slightly affect the heave estimate. No extension-related thickness variations are assumed, and line-length is preserved during extension.

For the physical models (Appendix A) from Withjack and Callaway (2000), the Top Sub-salt and the black marker bed within the supra-salt strata were used to estimate extension. Sensitivity testing was then undertaken to investigate the measurement error associated with fault-heave summation along pre-kinematic horizons in the physical models. In all cases, we found that the measurement error was not significant (c. $\pm 1\%$), and the error associated with cut-off projection (Appendix D) was also not significant (c. $\pm 1\%$). The value of extension between pre-kinematic horizons was minimal (c. $\pm 1\%$).

For the Halten Terrace, the Top Ror Formation and Top Sub-salt horizons (Fig. 6) were used to estimate extension, and the discrepancy between the two was quantified (Fig. 7). Here, fault heave was measured perpendicular to the dominant fault strike every 500 m along-strike, and summed to give a total fault heave along the horizon of interest. Similarly to the physical models, sensitivity testing was undertaken along the pre-kinematic horizons in seismic sections to investigate the uncertainty associated with measurement in section. We found that measured extension varied by c. $\pm 4\%$, and was very dependent on the projection of and final position of cut-offs (Appendix D), which is in turn dependent on the velocity model, and the complexity of faulting and folding (e.g. Judge and Allmendinger, 2011). Repeat measurements of the same horizon were undertaken to determine the measurement precision under the same velocity model etc., and varied by c. $\pm 2\%$. We also note that the value of extension changes between pre-kinematic horizons, but it was not significant (c. $\pm 2\%$).

2.2 Line-length

Horizontal extension was calculated for two pre-kinematic horizons (Fig. 6), one above and one below the salt on a series of sections. The initial, pre-extension width (l_0) of a unit was measured by unfolding the horizon of interest and summed to give a total, perpendicular to the fault strike every 1000 m. The present-day, post-extension width (l_1) was then measured along the same section. The amount of extension (e) was calculated by subtracting the pre-extension width from the final, post-extension width i.e. $e = l_1 - l_0$. The percentage of extension of the pre-extension width (E) was calculated using a ratio of the total horizontal extension to the pre-extension width i.e. $E = e / l_0$. The line-length method considers brittle (faulting) and ductile

(folding) deformation when estimating the initial length. No extension-related thickness variations are assumed, and line-length is preserved during extension.

For the physical models (Appendix A) from Withjack and Callaway (2000), the Top Sub-salt and the black marker bed within the supra-salt strata was used to estimate extension (Fig. 4). Given the measurement error associated with line-length in section, we undertook sensitivity testing to assess the degree of variability of extension values. We found that the amount of extension is not significantly affected by measurement (c. $\pm 1\%$). The value of measured extension also does not typically vary between horizons (c. $\pm 1\%$).

For the Halten Terrace, the Top Ror Formation and Top Sub-salt horizons were used to estimate extension (Fig. 6), and the discrepancy between the two was quantified (Fig. 7). In this case, a velocity model (Appendix C) is required as vertical and horizontal components of deformation are considered. Sensitivity testing was undertaken using a range of sub-salt velocities (c. 3 – 5 km/s), where well checkshots were not available, the percentage of extension (E) is not significantly affected ($\pm 2\%$); given sub-salt strata is predominantly faulted, the effect of fold amplitude on extension is negligible. To assess the likely measurement error associated with line-lengths in the Halten Terrace seismic sections, we measured the same pre-kinematic horizon several times; we found that extension values were not significantly impacted by measurement variations (c. $\pm 1\%$). We also compared extension estimates from several supra-salt pre-kinematic horizons, and found that although extension estimates did change, line-length derived extension values did not change significantly (c. $\pm 2\%$). In addition, decompaction using shale vs. sand compaction curves (Sclater and Christie, 1980) may lead to variations of extension (c. $\pm 1\%$) as the horizon line-length changes.

2.3 Line-length vs. fault-heave errors

We found that extension estimates derived from fault-heave are less precise and less accurate compared to a line-length approach when taking into account measurement issues in both physical models and seismic. Decreased precision and accuracy associated with the fault-heave method may be largely attributed with the difficulty of projecting cut-offs (Appendix D) in areas where extension is accommodated as complex folding as well as faulting. Although beyond the scope of this study, this would be exacerbated between the same seismic data in time vs. depth given the cut-offs may be projected differently. In contrast, line-length requires no such projection (except when accounting for significant footwall erosion), and instead, assumes the line-length remains unchanged during extension. Furthermore, there are fewer opportunities for the interpreter to make errors in a line-length approach relative to fault-heave summation.

Calculated errors for estimate extension associated with each method in the physical models and the Halten Terrace, offshore Norway.

Source of error	Extension error in Withjack & Callaway models	
	Line-length	Fault-heave
Measurement error	$\pm 1\%$	$\pm 1\%$
Cut-off projection	N/A	$\pm 1\%$
Choice of horizon	$\pm 1\%$	$\pm 1\%$
Cumulative error	$\pm 2\%$	$\pm 3\%$

Source of error	Extension error in Halten Terrace	
	Line-length	Fault-heave
Measurement error	± 1%	± 2%
Cut-off projection	N/A	± 4%
Choice of horizon	± 1%	± 2%
Velocity model	± 2%	Included in cut-off
Decompaction	± 1%	N/A
Cumulative error	± 5%	± 8%

2.4 Oblique fault strikes relative to transport direction

In the hypothetical case where heave is measured on faults striking obliquely to the transport direction, heave may be overestimated. To estimate the potential errors, we explore the following scenario.

For a fault dipping at 70°, similar to the Halten Terrace faults, with a maximum throw of 100 m, heave can be calculated as ~36 m. As the section becomes more oblique, the dip of the fault will change. Our estimates show a difference between sub- and supra-salt average strikes as <10° (Fig. 7), and no greater than 30°. Hence, when measuring heave at different values of obliquity, the heave varies as follows:

Obliquity	Calculated heave	Difference	Overestimation error
None	36 m	0 m	N/A
10°	37 m	1 m	2.7%
20°	39 m	2 m	5.6%
30°	42 m	6 m	16.7%

If the discrepancy between all of the sub- and supra-salt faults is < 30°, then heave may have been overestimated by 16% of the calculated extension value i.e. 0.16 x extension. As the sections used to calculate extension are perpendicular to the largest, dominant fault strike, the overestimate of heave is only likely on the relatively small faults, which are unlikely to significantly affect our results, and especially compared to the cumulative errors in the prior section.

3. Structural restoration of the Halten Terrace

To validate our interpretation of the seismic horizons in the Halten Terrace, we undertake structural restoration, following the procedure outlined in Lingrey and Vidal-Royo (2015) and Rowan and Ratliff (2012) using Midland Valley's Move software (Appendix F). We chose a line of section oriented perpendicular to the regional strike of major faults and folds, and the major transport direction. We interpreted regional horizons (Fig. 5) and assigned lithological information, based upon local well information, to each stratigraphic interval and then sequentially decompacted the supra-salt overburden using compaction curves from the North Sea (Sclater and Christie, 1980). When appropriate we restored supra-salt fault blocks using rigid body rotation, making the uppermost layers subparallel to the sub-horizontal datum. Rotation was followed by unfolding of the layers using inclined shear; the shear angle was

chosen via trial and error, by finding the angle that provides the least variations in the area and layer shape. The shear inclination is typically antithetic to the fault dip, and chosen angles range between 60 and 75°, and may vary between fault blocks. When fault blocks are translated and gathered, areas of mismatch are aligned as such that the area of the gap is roughly equal to the area of overlap (after Lingrey and Vidal-Royo, 2015). These gaps will either lead to an underestimate the extension if no overlap occurs, or an overestimate if the overlap is too great. Once the basins have been translated and unfolded, the next layer is decompacted. The process is repeated until the supra-salt layers have been successively restored. Given the close vertical spacing within the relatively thin Jurassic interval (Appendix B), some horizons have been omitted from the restoration.

The movement of sub-salt faults is poorly constrained, however, the hard-linked fault joining the sub-salt and supra-salt strata is used to infer the movement of the sub-salt. By removing the throw along the hard-linked fault at the supra-salt level, the throw at the sub-salt level is also removed. To calculate the remaining position of the sub-salt faults, the sub-salt blocks undergo rigid body rotation (as with the supra-salt) and are translated. The area of the salt is maintained throughout the restoration as the salt is relatively immobile in the Halten Terrace, although in reality salt likely flows in and out of the section. Once the supra-salt units have been reconstructed to the Mid Jurassic (and the Intra Åre Fm is restored to sub-horizontal), the sub-salt fault blocks are unfolded using inclined shear.

The line-length variation between the present-day and restored section is minimal (< 2%). We find that once the sub-salt is fully restored, the sub-salt line-length is very similar (~ 660m difference) to that of the supra-salt (Intra Åre Fm) i.e. sub- and supra-salt extension is balanced, indicative of kinematic coherence.

Supra-salt values for extension derived from line-length may vary dependent on decompaction in the restoration procedure described above ($\pm 1\%$ between shale and sand decompaction trends; Section 2.3). Decompaction also strongly influences the in-section area of the units throughout the restoration process, leading to < 60% area variations between the deformed, present-day state vs. the restored state.

A table compiling the linear strain stretch values for the Top Ror, Intra Åre and Top Sub-salt horizons prior in its deformed state (prior to restoration) and restored (following decompaction, rigid block translation, and unfolding) is presented below:

Horizon	Deformed line-length (m)	Restored line-length (m)	Stretch ($1 + \Delta$)
Top Ror	21800	21170	0.989
Intra Åre	20810	21170	0.983
Top Sub-salt	21390	21830	0.980

To assess the quality of our block restoration and area balance, we followed the method of Lingrey and Vidal-Royo (2015). We compared the overlaps/gaps in the restoration following rigid block translation and decompaction of the overburden, to calculate the area mismatch i.e. the ratio of the “Decompacted area” with the “Net area of the gaps/overlaps”. The results are presented below:

Horizon	Decompacted area (m ²)	Net area of gaps/overlaps (m ²)	Areal mismatch (%)
Top Ror	2.21 x 10 ⁷	3.50 x 10 ⁵	0.49
Intra Åre	2.84 x 10 ⁷	6.62 x 10 ⁵	1.27
Top Sub-salt	7.29 x 10 ⁷	1.18 x 10 ⁶	1.62

Lingrey and Vidal-Royo (2015) suggest that good restorations should have areal mismatch values below 5%; when mismatch errors exceed 5%, the balance is considered poor and either the deformed state interpretation needs modification, different unfolding parameters/techniques need to be tried, or a geologic reason for the discrepancy needs to be offered. Our values, which are typically < 2% suggest that our interpretation is valid and can be considered balanced.

4. References cited in Appendix E

- Breivik, A. J., Faleide, J. I., Mjelde, R., and Flueh, E. R., 2009, Magma productivity and early seafloor spreading rate correlation on the northern Vøring Margin, Norway—constraints on mantle melting: *Tectonophysics*, v. 468, no. 1, p. 206-223.
- Breivik, A. J., Mjelde, R., Raum, T., Faleide, J. I., Murai, Y., and Flueh, E. R., 2011, Crustal structure beneath the Trøndelag Platform and adjacent areas of the mid-Norwegian margin, as derived from wide-angle seismic and potential field data: *Norwegian Journal of Geology*, v. 90, p. 141-161.
- Brown, A. R., 2001, Calibrate yourself to your data! A vital first step in seismic interpretation: *Geophysical Prospecting*, v. 49, no. 6, p. 729-733.
- Judge, P. A., and Allmendinger, R. W., 2011, Assessing uncertainties in balanced cross sections: *Journal of Structural Geology*, v. 33, no. 4, p. 458-467.
- Lingrey, S., and Vidal-Royo, O., 2015, Evaluating the quality of bed length and area balance in 2D structural restorations: *Interpretation*, v. 3, no. 4, p. SAA133-SAA160.
- Marsh, N., Imber, J., Holdsworth, R., Brockbank, P., and Ringrose, P., 2010, The structural evolution of the Halten Terrace, offshore Mid-Norway: extensional fault growth and strain localisation in a multi-layer brittle–ductile system: *Basin Research*, v. 22, no. 2, p. 195-214.
- Richardson, N. J., Underhill, J. R., and Lewis, G., 2005, The role of evaporite mobility in modifying subsidence patterns during normal fault growth and linkage, Halten Terrace, Mid-Norway: *Basin Research*, v. 17, no. 2, p. 203-223.
- Rowan, M. G., and Ratliff, R. A., 2012, Cross-section restoration of salt-related deformation: Best practices and potential pitfalls: *Journal of Structural Geology*, v. 41, p. 24-37.
- Sclater, J. G., and Christie, P., 1980, Continental stretching; an explanation of the post-Mid-Cretaceous subsidence of the central North Sea basin: *Journal of Geophysical Research*, v. 85, no. B7, p. 3711-3739.
- Stewart, S. A., Harvey, M. J., Otto, S. C., and Weston, P. J., 1996, Influence of salt on fault geometry: examples from the UK salt basins: Geological Society, London, Special Publications, v. 100, no. 1, p. 175-202.

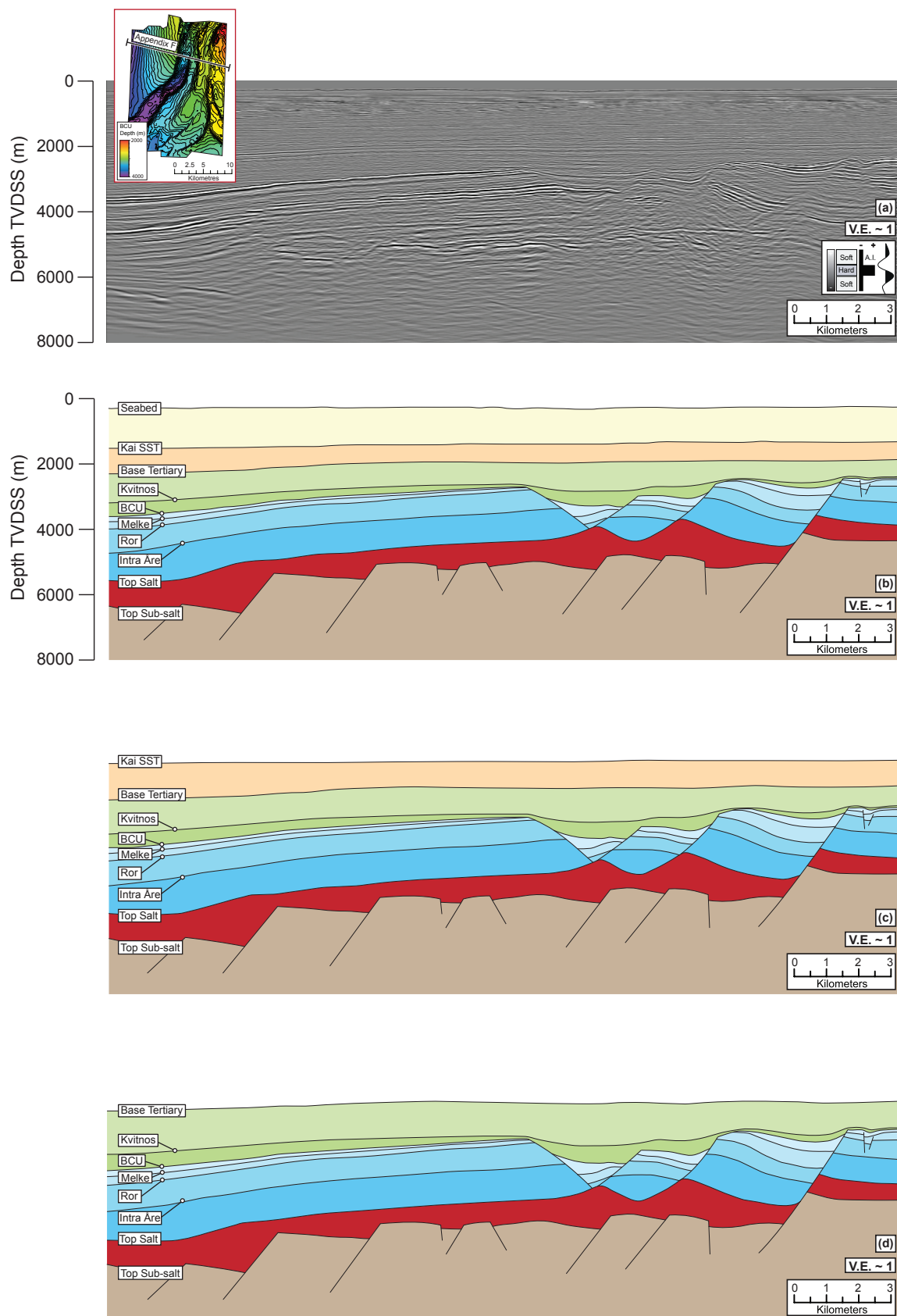
Storvoll, V., Bjørlykke, K., and Mondol, N. H., 2005, Velocity-depth trends in Mesozoic and Cenozoic sediments from the Norwegian Shelf: AAPG bulletin, v. 89, no. 3, p. 359-381.

Walsh, J. J., Watterson, J., Childs, C., and Nicol, A., 1996, Ductile strain effects in the analysis of seismic interpretations of normal fault systems: Geological Society, London, Special Publications, v. 99, no. 1, p. 27-40.

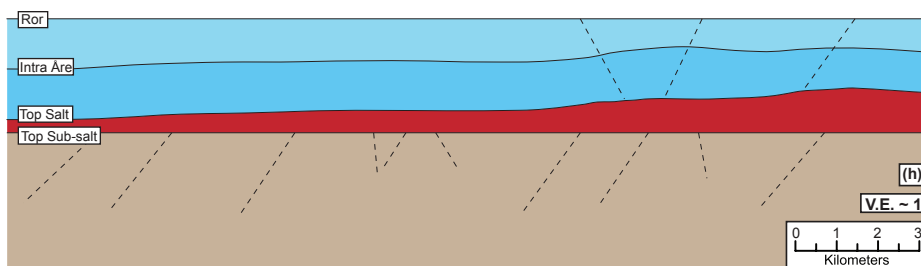
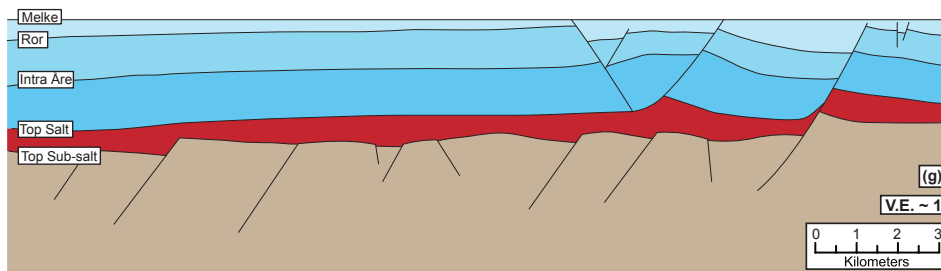
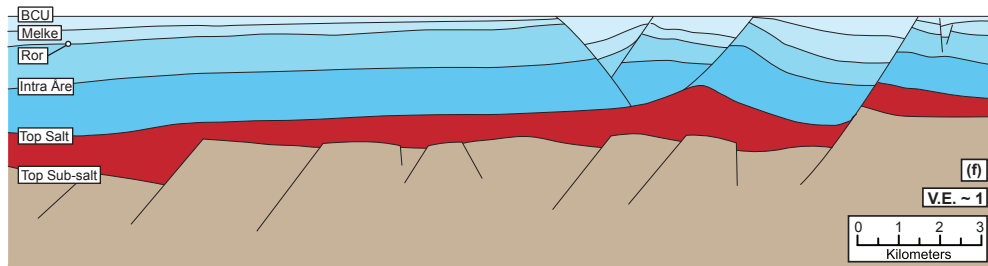
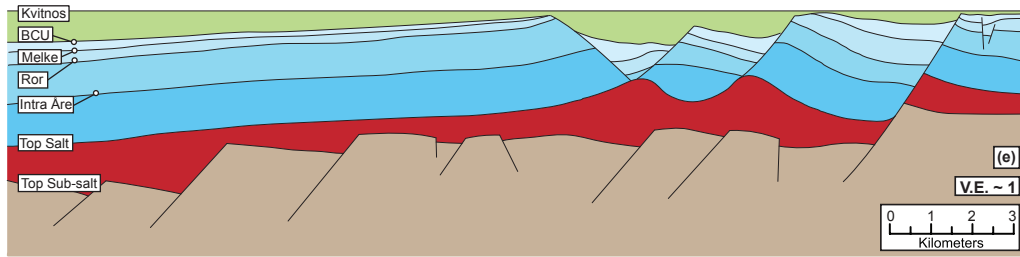
Wilson, P., Elliott, G. M., Gawthorpe, R. L., Jackson, C. A., Michelsen, L., and Sharp, I. R., 2015, Lateral variation in structural style along an evaporite-influenced rift fault system in the Halten Terrace, Norway: Influence of basement structure and evaporite facies: Journal of Structural Geology, v. 79, p. 110-123.

Wilson, P., Elliott, G. M., Gawthorpe, R. L., Jackson, C. A.-L., Michelsen, L., and Sharp, I. R., 2013, Geometry and segmentation of an evaporite-detached normal fault array: 3D seismic analysis of the southern Bremstein Fault Complex, offshore mid-Norway: Journal of Structural Geology, v. 51, p. 74-91.

Withjack, M. O., and Callaway, S., 2000, Active normal faulting beneath a salt layer: an experimental study of deformation patterns in the cover sequence: AAPG bulletin, v. 84, no. 5, p. 627-651.



Appendix F - Structural restoration for the Halten Terrace. (a) Uninterpreted 2D seismic reflection profile trending NW-SE through the 3D seismic volume. The location of the section is shown atop the BCU depth structure map. (b) Interpreted section used in Midland Valley's Move software for the structural restoration. (c) Restoration for the Kai SST horizon. (d) Restoration for the Base Tertiary horizon. The overburden has been decompacted, and the fault blocks have undergone rigid body rotation and translation to near horizontal. The horizon to be restored was then unfolded to horizontal using flexural slip. Sub-salt faults were not active during the Late Cretaceous - Tertiary. A constant area for the salt is assumed. For a full description of the structural restoration procedure, see Appendix E. The colours on the interpreted section are shown in Figure 5. All sections have been depth converted using the time-depth relationship in Appendix C.



Appendix F continued - Structural restoration for the Halten Terrace. (e) Restoration for the Kvitnos, (f) BCU, (g) Top Melke and (h) Top Ror horizons. The overburden has been decompacted, and the fault blocks have undergone rigid body rotation and translation to near horizontal. The horizon to be restored was then unfolded to horizontal using flexural slip. When the supra-salt faults are restored, the hard-linked fault (directly connecting the sub- and supra-salt strata) was backstripped, reconstructing fault activity to the east. The remaining sub-salt fault activity is poorly constrained so a constant area for the salt is assumed, however, our analysis shows the sub- and supra-salt faults are kinematically coherent hence are active at similar times. For a full description of the structural restoration procedure, see Appendix E. The position of future faults are shown as dashed lines. Line-length was measured on the restored section versus the original interpretation (Appendix E). Colours shown in Figure 5. All sections have been depth converted using the time-depth relationship in Appendix C.